Application of atom probe tomography to the investigation of atomic force microscope tips and interfacial phenomena

by

Christopher Joseph Tourek

A dissertation submitted to the graduate faculty

in partial fulfillment of the requirements for the degree of

DOCTOR OF PHILOSOPHY

Major: Mechanical Engineering

Program of Study Committee:

Sriram Sundararajan, Major Professor
Andrew Hillier
Pranav Shrotriya
Krishna Rajan
Gap-Yong Kim

Iowa State University

Ames, Iowa

2012

TABLE OF CONTENTS

ACKNOWLEDGEMENTS

First I would like to thank my advisor Dr. Sriram Sundararajan for all of the guidance and support that he has given me throughout the years. I am the researcher I am now because of him. He showed me that I not only needed to be persistent but also always mindful of how and why things are working. Without good planing and knowledge of the process you can't troubleshoot problems when they arise, and they will.

I would also like to extend my sincere thanks to the members of my committee: Dr. Andrew Hillier. Dr. Pranav Shrotriya, Dr. Krishna Rajan, and Dr. Gap-Yong Kim for serving on my committee and giving me advice and direction whenever I needed it. I would especially like to thank Dr. Hillier for not getting upset when I would come to tell him yet again that there was something not working right on the atom probe.

Thanks to all the staff in the ME department for none of us would be successful without their help.

I owe a big thank you to Dr. Steven Kawaler for allowing me to get a taste of how exciting and fun research is by helping in his group way back in my freshman year. I also would like to thank Dr. Curtis Mosher for always being willing to give a second opinion on why the AFM was acting weird, and I really appreciate all the conversations we had both relevant and non-relevant while my images were capturing.

A big acknowledgement goes out to my fellow grad students and friends with whom I have shared all the ups and downs that are a part of research; Satyam, KK, Rob, Srinath, Jing, Eric, Gilson, Reuben, Yilei, Mike, Dinesh, Santosh, Rupa, Joe, and Xiao. And to all my friends who are too numerous to list, but without whom my time in Ames would have been much less fun.

I would also like to thank Bethany for always being there, encouraging me and being a rock to calm me down in these last few months.

Last but not least I would like to thank my parents for their constant encouragement and unerring faith that I would succeed. Without their unconditional love and support I could not have accomplish what I have.

Financial support for this work was provided by grants from the National Science Foundation (Grant no. 0932573), the W.M. Keck Foundation, and Iowa State University.

ABSTRACT

This dissertation demonstrates the research effort to extend the analytical capabilities of atomic force microscopy (AFM) by utilizing atom probe tomography (APT) to investigate AFM tips for the first time. Novel techniques were developed to enable successful analysis of various AFM tips and layers created on the tips. Initial investigations focused on comparing results obtained from as received Si AFM tips to a standard Si APT sample. It was found that by using careful alignment and stiffer cantilevers (>25N/m) AFM tips are readily analyzable by APT. The techniques were then applied to commercially available coated Si AFM tips and high aspect ratio metallic needle tips to demonstrate the broad applicability. A new method to calibrate the optical sensitivity of AFM cantilevers was developed to eliminate damage to the AFM tip. Finally the new calibration method was utilized in the investigation of transferred material from AFM sliding experiments. It was found that the transferred material was readily detected and characterized. The successful results demonstrate the ability of APT application to AFM tips enhancing the information from AFM experiments and opening new areas of investigation.

CHAPTER 1. INTRODUCTION

The overarching theme of this dissertation research is to utilize atom probe tomography to further the application of atomic force microscopy. This introductory chapter outlines the background, motivation and objectives of the research work.

1.1 Background

1.1.1 Atomic force microscopy

Atomic force microscopy (AFM) is a widely used technique that is part of the scanning probe microcopy family. The original scanning probe microscope is the scanning tunneling microscope (STM) developed in 1981 by Binnig and Rohrer [1] who later received the 1986 Nobel Prize in Physics for their inventing of the STM. It operates by moving a sharp tip into close proximity with the sample's surface and creating a bias between the two. When the tip is close enough to the surface the bias will induce quantum mechanical tunneling of electrons across the void. The tunneling current is exponentially dependent on the distance between the tip and the sample. As the tip is rastered across the surface the tunneling current between the tip and sample is monitored and a feedback loop is utilized to keep the current constant. This results in keeping the tip a constant distance above the sample and can give a topological map of the surface. While this technique is quite powerful and since its invention has been

utilized to image individual surface atoms, it is restricted to conductive samples and must be conducted in vacuum.

One of the key developments from STM is the ability to stabilize and scan a fine probe over a sample surface to nanometer accuracies by using piezoelectric scanners and a feedback loop. These principles were used by Binnig, Quate, and Gerber in 1986 to create the first AFM [2]. In the first AFM a STM was used to monitor the deflection of a cantilever with a sharp tip attached that is in contact with the surface. By using the AFM tip to interact with the surface instead of the STM it was now possible to analyze non-conductive samples. The next great step in instrumentation introduced using a laser beam reflected off the backside of the AFM cantilever to monitor its deflection [3] thus eliminating the need for using a STM to monitor the deflection. Therefore experiments could be done on both conducting and non-conducting samples in air, gas, vacuum or liquid greatly increasing the number of samples and experimental conditions that can be investigated.

The AFM measures the small forces between a sharp tip at the end of a cantilever and the surface of a sample and is capable of sub-nanometer resolution. An example of an AFM tip and cantilever is shown in Figure 3. The sharp tip and cantilever assembly is mounted opposite the sample to be investigated with either the tip or the sample able to be moved by a piezoelectric tube to allow sub-nanometer positioning. A laser beam is aligned and focused to

reflect off the backside of the cantilever and onto a photodiode (photodetector). Then as the piezo rasters the tip relative to the sample the cantilever will bend and twist in response to interaction forces with the sample causing the laser to move on the photodetector. This signal is used to allow the AFM to track the surface as well as determine information about the tip's interaction with the surface.

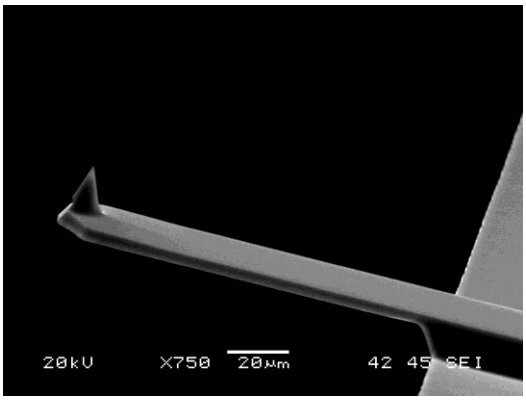

Figure 3. An example of an AFM tip and cantilever attached to a chip for ease of handling.

The most basic mode of AFM keeps the tip in constant contact with the surface by maintaining a continuous deflection of the cantilever (contact mode). The operating principles are shown in Figure 4. As the tip is rastered across the surface topographical features cause the cantilever to deflect away from the desired setpoint moving the corresponding laser spot on the photodetector. In a four quadrant photodetector the vertical signal is found by subtracting the bottom

two quadrants from the top, (A+B)-(C+D) in Figure 4. This signal is used in a feedback loop to adjust the voltage to the piezo and thus return to the set deflection point. By recording the changes in voltage to the piezo a topographical map of the surface can be generated. If the spring stiffness of the cantilever and the motion of the laser on the photodetector are known then the force applied to the sample can be calculated and set. Also as the tip is in constant contact with the surface if it is moved perpendicular to the long axis of the cantilever the interactions with the sample will cause a twisting of the cantilever. As the cantilever twists the laser will move sideways on the photodetector giving information about the friction between the tip and surface.

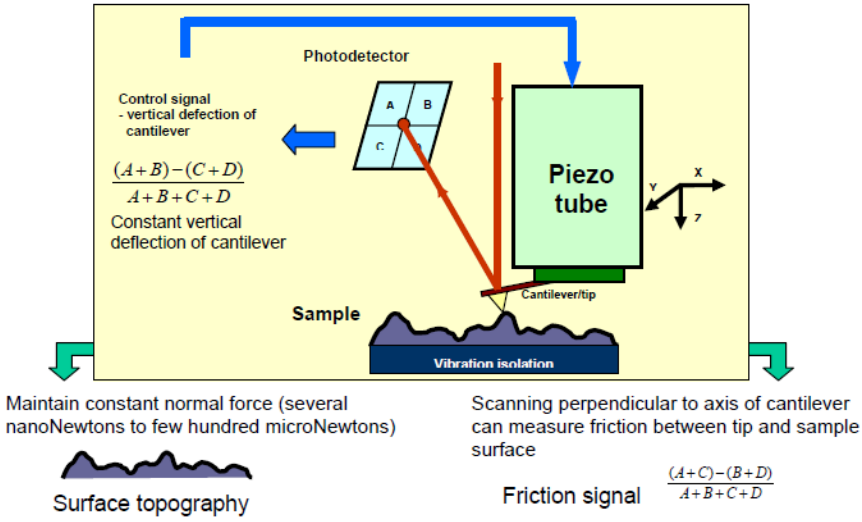

Figure 4. Operating principles of contact mode atomic force microscopy (AFM)

To control the force applied by the tip in contact mode two quantities need to be found. First, the spring stiffness of the cantilever needs to be determined. Manufactures quote spring stiffness for their cantilevers, but they can be incorrect by as much as 100%. Therefore it is necessary to calibrate each cantilever when the force applied during the experiment is vital. The method used in this work was developed by Sader et al. [4]. It calculates the spring constant by using the density and viscosity of the fluid surrounding the cantilever along with the planar dimensions, resonant frequency and dampening of the cantilever. The planar dimensions of the cantilever were found from optical microscopy and the resonant frequency and dampening was found using the commercial AFM software used in the experiments (Nanoscope, Bruker). The second quantity needed is the relationship between the bending of the cantilever and the movement of the laser spot on the photodetector. Commonly known as the optical sensitivity. A novel way to calibrate this quantity is detailed in Chapter 5. It utilizes a tungsten spike to contact the cantilever away from the AFM tip to cause the cantilever to bend to determine the optical sensitivity. This technique prevents damage to the AFM tip.

A second common mode of operation of the AFM is termed intermittent contact mode or tapping mode [5]. Here the cantilever is vibrated at a set amplitude and as it interacts with the surface the amplitude will change. By using the change in amplitude in a feedback loop, similar to contact mode, the tip can track the surface. An advantage to tapping mode is virtually no lateral force on

the tip and the vertical force applied to the tip is less than in contact mode. This facilitates the use of sharper tips as there is less likelihood of breakage from interactions with the surface.

AFM has become one of the most powerful tools for preparation and analysis of material's surfaces and their functionality [6-13]. Since its invention a whole family of techniques and applications has been generated based on the principles of AFM. The following are examples of the characterization techniques that have grown from AFM. A first example is electrical force microscopy in which a conductive tip can be used to characterize the electrical properties of micro and nanoscale electronic devices [14-16]. This technique is of great importance as electronics manufacturing in the silicone semiconductor industry has progressed to the nanometer scale. Another example which has been applied extensively to aid in the development and application of magnetic based recording components is magnetic force microscopy where a magnetic tip is used to sense magnetic domain changes in the sample [17-19]. Nanoindentaion is a third technique where the AFM tip is used to damage the surface to determine material properties of the sample [20-22]. A final example is scanning probe lithography where the tip is used to manipulate the nanostructure of the surface. Specific examples include mechanical indentation, plowing, nanomanipulation, dip-pen nanolithography, anodic oxidation, electrochemical deposition, and nanoscale explosion [23-25]. Figure 5 shows an image of one of the most popular

demonstrations of nanolithography, the Mona Lisa, crated by a style of diamond like carbon (DLC) coated AFM tip that is analyzed in Chapter 4.

Figure 5. Nanolithography image of the Mona Lisa [26].

1.1.2 Atom Probe Tomography

Atom probe tomography (APT) is a technique capable of concurrently determining three-dimensional material structure and chemistry at near atomic resolution [27]. It was developed from the field emission microscope (FEM) and field ion microscope (FIM). The first FEM was invented in 1936 by E. W. Mueller at Technical University of Berlin, Germany [28]. It utilized a negative potential to emit electrons normal to the surface of a sharp metallic needle. The electrons

were projected onto a phosphor screen to form an image, and it was able to achieve a special resolution of 2nm.

FIM, invented by Bahadur and Müller at Pennsylvania State University on October 1955, was the first technique to achieve an image of individual atoms [27, 29]. A sharp tungsten needle was cooled to cryogenic temperatures and given a positive bias. An imaging gas was introduced into the chamber and the voltage was regulated so that the gas near the surface of the tip would field ionize by quantum mechanical tunneling under the high electric field. The ions would then be repelled by the positively charged tip and follow the field lines toward a phosphorus screen to create an image showing a projection of the arrangement of the surface atoms of the tip.

In both FIM and FEM the surface atoms generally don't leave the surface, and in fact it is usually undesirable. In 1956 Müller made the discovery of field evaporation [27]. Field evaporation is the phenomena of surface atoms subliming from a material's surface in the presence of a high field. By careful control of the field atoms can be removed in an orderly fashion. In 1967 and 1968, Müller and Panitz created the first atom probe microscope by adding a mass spectrometer to a FIM to identify the composition of the sample atoms that were field evaporated [30]. In most early atom probe microscopes voltage pulses were used to field ionize the sample, however this approach will only work for conductive materials. In the 1970s researchers explored using laser pulses to

assist in the field evaporation process [31]. Originally work was slow, but recently with increasing desire to investigate semiconducting and insulating materials fast laser pulsing systems have been developed [32, 33]. The first commercially available pulsed laser atom probe microscope was developed in 2002 by Imago (now Cameca) [34].

Early atom probe microscopes utilized oscilloscopes to monitor the detection of atoms and had no positional information [27]. In the 1980s atom probe microscopes were fitted with position sensitive detectors and with the aid of computers a three dimensional image could be constructed from the detected ions [35, 36]. Therefore the technique is now commonly referred to as atom probe tomography (APT). The most recent advance in APT was the incorporation of the local electrode which significantly reduces the voltage needed for field evaporation [37, 38]. The commercially available local electrode atom probe (LEAP) utilizes a local electrode along with incorporating both voltage and laser pulsing to increase its ability to analyze more materials.

Analysis in APT can be divided into two separate steps. First is the experiment where ions are field evaporated and detected, and second the reconstruction. In the reconstruction the original atomic positions and identities are determined by the hit order and position on the detector along with the time of flight information about the hit from the mass spectrometer. Both parts of APT are described in detail below.

The APT experiment portion works on the phenomena of field evaporation, by which surface atoms of the specimen are ionized in ultra-high vacuum and subsequently desorbed by an electric field [29]. A diagram for a model of the field ionization process is shown in Figure 6. The barrier for an atom to ionize and evaporate is strongly reduced by the presence of an electric field as the Schottky hump ($Q_n(\mathbf{E})$) gets reduced allowing the atom to ionize [39]. Ultra high vacuum on the order of 10^{-11} Torr is utilized in atom probe microscopes to limit interactions of the field evaporated ions with anything on their flight to the detector as deviations in flight path will impact the accuracy of the reconstruction. A schematic of the APT instrumentation is shown in Figure 7. The field evaporation process is controlled by utilizing a cryogenically cooled needle-shaped specimen. Cryogenic cooling is used to reduce atomistic vibrations and analysis is typically performed at 20-100K. The sharp needle shape is used to increase the electric field magnitude for evaporation and is on the order of 10s of nanometers. The specimen is kept at a standing voltage while a local electrode is given a pulsed voltage or the tip of the specimen is given a laser pulse in order to incite controlled field evaporation. The standing voltage on the sample is kept close to the voltage needed for field evaporation, and the voltage or laser pulse is used to increase the field just enough to induce one atom to field evaporate. The ionized atom is then repelled by the electric field through a hole in the local electrode towards a microchannel plate (MCP) that releases a cascade of electrons on the ion impact. The electrons hit a wide-angle position-sensitive

detector equipped with a time-of flight mass spectrometer with single atom sensitivity. This process is repeated until either a suitable amount of ions are detected or the specimen fractures. Typical pulse rates for modern atom probe microscopes are in the hundreds of thousands of hertz, but only a small portion of pulses induce a field evaporation event leading to collection rates of 1000s of ions a second.

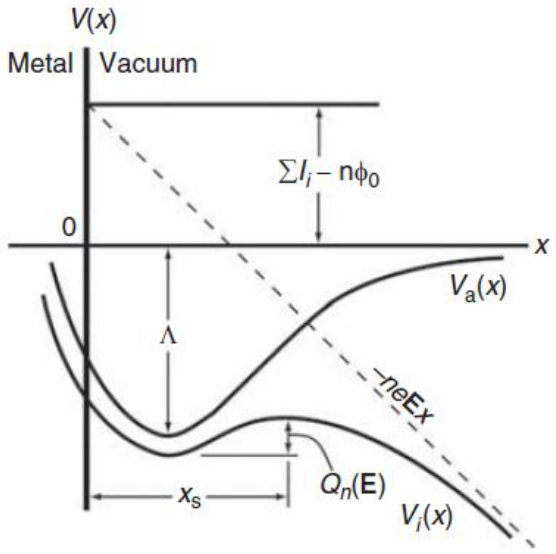

Figure 6. *V(x)* is potential energy as a function of distance away from the surface of a specimen, $x = 0$. $V_a(x)$ is the potential energy of an atom in the absence of an electric field, **E**, and $V_i(x)$ is the potential energy of an ion in its ith ionization state in the presence of E. I_i is the *i*th ionization state of an ion, *e* is the charge on an electron, *n* is the number of electronic charges, Λ is the cohesive energy of a solid, φ_0 is the local work function, $Q_n(\mathbf{E})$ is the height of the so-called Schottky hump, and x_s is the position of the maximum value of the Schottky hump.

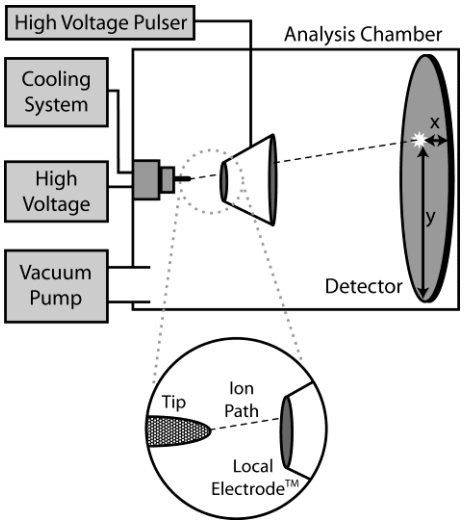

Figure 7. Diagram of an atom probe microscope.

The second part of APT is reconstructing the ion's original positions. Most current reconstruction algorithms are based on the work of Bas et al. [40]. First the raw hit information is adjusted to account for the curvature of the tip and changes in voltage through the run. These corrections are usually done iteratively until the change between iterations reaches a threshold. The lateral coordinates of the ions are calculated from the recorded impact position on the detector and a magnification factor determined by:

$$M = \frac{D}{d} = \frac{L + \xi R}{\xi R} \cong \frac{L}{\xi R} \tag{1}$$

where M is the magnification, D is the distance from the center of the detector to the ion impact point, d is the distance from the specimen axis and the projection of the ion into the plane tangent to the specimen apex, L is the distance from the detector to the tip, R is the tip radius, and ξ is the image compression factor.

As field evaporation proceeds the tip radius will increase as the atoms on the upper part of the tip are field evaporated. This will change the magnification as the experiment progresses. To account for this two methods can be utilized. First the tip radius for each ion can be calculated from the equation for the field at the tip:

$$F = \frac{V}{kR} \tag{2}$$

where F is the field necessary to field evaporate the ion, V is the voltage on the tip, and k is a geometric factor commonly known as the field factor to account for deviation of the electric field from that of a sphere. The second way to determine the evolution of the tip radius is to impose a shank angle to the reconstruction.

The depth coordinate can be found assuming the atomic volume is distributed homogeneously across the analyzed area and ions originate from an emitting surface. As ions are evaporated from the tip the specimen becomes farther from the original surface. Therefore for each ion added to the reconstruction the emitting surface is incrementally shifted by a small quantity:

$$dz = \frac{\Omega L^2}{\eta A_d \xi^2 R^2} \tag{3}$$

where dz is the depth increment, Ω is the volume of the ion, L is the distance from tip to detector, η is the efficiency of the detector, A_d is the area of the detector, ξ is the image compression factor, and R is the tip radius. To account for the curvature of the tip a correction is applied:

$$dz' = R_i \left(1 - \sqrt{1 - \frac{x_i^2 + y_i^2}{R_i^2}} \right) \tag{4}$$

Where R_i is the radius of the tip when ion *i* is evaporated and x_i and y_i are the hit positions on the detector. Thus the *z* position of the ion is calculated by sequentially cumulating the depth increment and adding the corrective term:

$$z_i = \left(\sum_{1}^{i} dz \right) + dz_i' \tag{5}$$

Finally, the spatial coordinates of each atom are combined with its elemental identity from the time of flight spectrometer data to create a 3D computer reconstruction of the analyzed region of the sample. Typical magnifications of the specimen at the detector in most APT instruments are about 5-6 million times. Spatial resolution is limited by small trajectory aberrations of the ions close to the specimen surface and is typically ~0.2 nm laterally and ~0.05 nm in the depth coordinate [41].

As a comparison, energy filtering transmission electron microscopy (EFTEM) can provide two-dimensional chemical mapping with about 1 nm lateral resolution, which is limited by signal to noise issues [42]. A direct comparison of identical calibration structures demonstrated that the spatial resolution of the local chemical analysis by APT exceeds that of the unprocessed EFTEM by a factor of 2 [43]. Thus APT is one of the highest resolution three dimensional nanoscale analysis tools presently available.

1.2 Motivation and Objectives

As technological devices have greatly reduced in size in the past few decades the ability to investigate materials on the nanoscale becomes ever more important. This is especially pertinent with the advent of MEMs and NEMs. It has been shown above that AFM is a technique widely used in the fields of nanoscience for the preparation and analysis of materials, nanostructures and their functionality. In its application the interaction of the tip apex with the sample is vitally important. However detailed assessment of the structure and chemistry of the near apex region is difficult due to the geometry and length scale. On the other hand this same geometry and length scale make AFM tips potential samples for APT, and by applying APT to analyze AFM tips a wealth of new knowledge about nanoscale phenomenon can be gathered. One area that can greatly benefit from this analysis is nanotribology, which is the study of friction,

adhesion, lubrication and wear at contacts of nanometer sizes. There has been much work done to characterize what happens on the substrate side of a wear test, but quantitative investigation of the apex region of the tip side is lacking.

With this in mind, the research objectives of this dissertation are the following:

1 Demonstrate the ability to analyze AFM tips utilizing APT.

2 Utilize the technique to examine commercially available modified and novel AFM tips.

3 Apply the method to investigate material transfer onto AFM tips from sliding experiments.

1.3 Dissertation Organization

Following the introduction chapter, Chapter 2 reports on initial investigations of AFM tips using APT. In Chapter 3 the oxide layer on as received Si AFM tips is shown to be readily seen in laser pulsed APT. Chapter 4 expands the investigation of AFM tips to commercially available modified and novel tips.

A new way to calibrate the force applied in AFM studies is demonstrated in Chapter 5. Chapter 6 uses the new calibration in the investigation of transferred material from sliding experiments conducted using AFM.

References

1. Binnig, G. and H. Rohrer, SCANNING TUNNELING MICROSCOPY. Helvetica Physica Acta, 1982. 55(6): p. 726-735.

2. Binnig, G., C.F. Quate, and C. Gerber, ATOMIC FORCE MICROSCOPE. Physical Review Letters, 1986. 56(9): p. 930-933.

3. Alexander, S., et al., AN ATOMIC-RESOLUTION ATOMIC-FORCE MICROSCOPE IMPLEMENTED USING AN OPTICAL-LEVER. Journal of Applied Physics, 1989. 65(1): p. 164-167.

4. Sader, J.E., J.W.M. Chon, and P. Mulvaney, Calibration of rectangular atomic force microscope cantilevers. Review of Scientific Instruments, 1999. 70(10): p. 3967-3969.

5. Zhong, Q., et al., FRACTURED POLYMER SILICA FIBER SURFACE STUDIED BY TAPPING MODE ATOMIC-FORCE MICROSCOPY. Surface Science, 1993. 290(1-2): p. L688-L692.

6. Bhushan, B., J.N. Israelachvili, and U. Landman, NANOTRIBOLOGY - FRICTION, WEAR AND LUBRICATION AT THE ATOMIC-SCALE. Nature, 1995. 374(6523): p. 607-616.

7. Carpick, R.W. and M. Salmeron, Scratching the surface: Fundamental investigations of tribology with atomic force microscopy. Chemical Reviews, 1997. 97(4): p. 1163-1194.

8. Greene, M.E., et al., Application of scanning probe microscopy to the characterization and fabrication of hybrid nanomaterials. Microscopy Research and Technique, 2004. 64(5-6): p. 415-434.

9. Hansma, H.G. and L. Pietrasanta, Atomic force microscopy and other scanning probe microscopies. Current Opinion in Chemical Biology, 1998. 2(5): p. 579-584.

10. Lillehei, P.T. and L.A. Bottomley, Scanning probe microscopy. Analytical Chemistry, 2000. 72(12): p. 189R-196R.

11. Loos, J., The art of SPM: Scanning probe microscopy in materials science. Advanced Materials, 2005. 17(15): p. 1821-1833.

12. Oesterschulze, E., Recent developments of probes for scanning probe microscopy, in Advances in Imaging and Electron Physics, Vol 1182001. p. 129-206.

13. Poggi, M.A., et al., Scanning probe microscopy. Analytical Chemistry, 2004. 76(12): p. 3429-3443.

14. Berger, R., et al., Electrical Modes in Scanning Probe Microscopy. Macromolecular Rapid Communications, 2009. 30(14): p. 1167-1178.

15. Gewirth, A.A. and B.K. Niece, Electrochemical applications of in situ scanning probe microscopy. Chemical Reviews, 1997. 97(4): p. 1129-1162.

16. Kronik, L. and Y. Shapira, Surface photovoltage phenomena: theory, experiment, and applications. Surface Science Reports, 1999. 37(1-5): p. 1-206.

17. Gruverman, A. and A. Kholkin, Nanoscale ferroelectrics: processing, characterization and future trends. Reports on Progress in Physics, 2006. 69(8): p. 2443-2474.

18. Hartmann, U., Magnetic force microscopy. Annual Review of Materials Science, 1999. 29: p. 53-87.

19. Kalinin, S.V., et al., Nanoscale electromechanics of ferroelectric and biological systems: A new dimension in scanning probe microscopy. Annual Review of Materials Research, 2007. 37: p. 189-238.

20. Petzold, M., et al., APPLICATION OF ATOMIC-FORCE MICROSCOPY FOR MICROINDENTATION TESTING. Thin Solid Films, 1995. 264(2): p. 153-158.

21. Bhushan, B. and V.N. Koinkar, NANOINDENTATION HARDNESS MEASUREMENTS USING ATOMIC-FORCE MICROSCOPY. Applied Physics Letters, 1994. 64(13): p. 1653-1655.

22. VanLandingham, M.R., et al., Nanoindentation of polymers: An overview. Macromolecular Symposia, 2001. 167: p. 15-43.

23. Holmberg, K., H. Ronkainen, and A. Matthews, Tribology of thin coatings. Ceramics International, 2000. 26(7): p. 787-795.

24. Wouters, D. and U.S. Schubert, Nanolithography and nanochemistry: Probe-related patterning techniques and chemical modification for nanometer-sized devices. Angewandte Chemie-International Edition, 2004. 43(19): p. 2480-2495.

25. Xie, X.N., et al., Nanoscale materials patterning and engineering by atomic force microscopy nanolithography. Materials Science & Engineering R-Reports, 2006. 54(1-2): p. 1-48.

26. NT-MDT, AFM Probes and Accessories Catalogue, 2012.

27. Miller, M.K., Atom Probe Tomography Analysis at the Atomic Level2000, New York: Kluwer Academic/Plenum Publishers.

28. Müller, E.W., Zh. Tekh. Fiz, 1936(17): p. 412.

29. Muller, E.W. and K. Bahadur, FIELD IONIZATION OF GASES AT A METAL SURFACE AND THE RESOLUTION OF THE FIELD ION MICROSCOPE. Physical Review, 1956. 102(3): p. 624-631.

30. Muller, E.W., J.A. Panitz, and S.B. McLane, ATOM-PROBE FIELD ION MICROSCOPE. Review of Scientific Instruments, 1968. 39(1): p. 83-&.

31. Tsong, T.T., et al., PHOTON STIMULATED FIELD-IONIZATION. Journal of Chemical Physics, 1976. 65(6): p. 2469-2470.

32. Gault, B., et al., Design of a femtosecond laser assisted tomographic atom probe. Review of Scientific Instruments, 2006. 77(4).

33. Miller, M.K., IMPLEMENTATION OF THE OPTICAL ATOM PROBE. Surface Science, 1992. 266(1-3): p. 494-500.

34. Kelly, T.E., et al. First data from a commercial local electrode atom probe (LEAP). in Microscopy and Microanalysis 2002 Meeting. 2002. Quebec City, Canada: Cambridge Univ Press.

35. Miller, M.K., CONCEPTS IN ATOM PROBE DESIGNS. Surface Science, 1991. 246(1-3): p. 428-433.

36. Nishikawa, O. and M. Kimoto, TOWARD A SCANNING ATOM-PROBE - COMPUTER-SIMULATION OF ELECTRIC-FIELD. Applied Surface Science, 1994. 76(1-4): p. 424-430.

37. Kelly, T.E., et al., First data from a commercial local electrode atom probe (LEAP). Microscopy and Microanalysis, 2004. 10(3): p. 373-383.

38. Kelly, T.F., et al., On the many advantages of local-electrode atom probes. Ultramicroscopy, 1996. 62(1-2): p. 29-42.

39. Seidman, D.N. and K. Stiller, An Atom-Probe Tomography Primer. Mrs Bulletin, 2009. 34(10): p. 717-724.

40. Bas, P., et al., A GENERAL PROTOCOL FOR THE RECONSTRUCTION OF 3D ATOM-PROBE DATA. Applied Surface Science, 1995. 87/88: p. 298-304.

41. Miller, M.K., Interface analysis with the three-dimensional atom probe. Surface and Interface Analysis, 2001. 31(7): p. 593-598.

42. Grogger, W., et al., Energy-filtering TEM at high magnification: spatial resolution and detection limits. Ultramicroscopy, 2003. 96(3-4): p. 481-489.

43. Stender, P., et al., Quantitative comparison of energy-filtering transmission electron microscopy and atom probe tomography. Ultramicroscopy, 2009. 109(5): p. 612-618.

CHAPTER 2. ATOM SCALE CHARACTERIZATION OF THE NEAR APEX REGION OF AN ATOMIC FORCE MICROSCOPE TIP

Modified from a paper published in Microscopy and Microanalysis

Christopher J. Tourek, Sriram Sundararajan

2.1 Abstract

3D atom probe tomography (APT) is successfully used to analyze the near-apex regions of an atomic force microscope (AFM) tip. Atom scale material structure and chemistry from APT analysis for standard silicon AFM tips and silicon AFM tips coated with a thin film of Cu is presented. Comparison of the thin film data with that observed using transmission electron microscopy indicates that APT can be reliably used to investigate the material structure and chemistry of the apex of an AFM tip at near atomic scales.

2.2 Introduction

Since its invention in the early 1980s atomic force microscopy (AFM) or scanning probe microscopy (SPM) has become one of the most powerful tools in the fields of nanoscience and nanotechnology for the preparation and analysis of materials, nanostructures and their functionality (Bhushan, et al., 1995; Carpick &

Salmeron, 1997; Greene, et al., 2004; Hansma & Pietrasanta, 1998; Lillehei & Bottomley, 2000; Loos, 2005; Oesterschulze, 2001; Poggi, et al., 2004). Over the years, the basic principle of SPM – measuring a specific interaction between an ultra-sharp tip and a material's surface to collect structural or functional information, has generated a complete family of techniques such as electrical force microscopy, (Berger, et al., 2009; Gewirth & Niece, 1997; Kronik & Shapira, 1999) magnetic force microscopy (Gruverman & Kholkin, 2006; Hartmann, 1999; Kalinin, et al., 2007) and scanning probe lithography, (Holmberg, et al., 2000; Wouters & Schubert, 2004; Xie, et al., 2006) to name a few. Using specific tips and measuring conditions, a whole range of data can be measured (Butt, et al., 2005; Giancarlo & Flynn, 1998; Horber & Miles, 2003; Magonov & Reneker, 1997; Muller & Dufrene, 2008; Nicholls, et al., 2005; Samori, 2004; Santos & Castanho, 2004). Analyzing the geometry of the near apex region of the AFM tip can provide useful information for various applications including investigation of modified probes (e.g. nanotube attachments) (Cheung, et al., 2000; Martinez, et al., 2005; Wade, et al., 2004) or for in-situ analysis of tip shape during experiments (Fujisawa & Kizuka, 2003). Detailed assessment of the structure and chemistry of the near apex region of the AFM tip can greatly expand the analysis capabilities afforded by AFM. Specific areas include fabrication and wear using AFM tips where material transfer and tip chemistry are of importance (Chung & Kim, 2007; Karuppiah, et al., 2009a; Karuppiah, et al., 2009b; Tanaka,

et al., 2009). To our knowledge, such analysis of AFM tips have not been reported in the literature.

This paper presents the results of a study aimed at using three-dimensional atom probe tomography (APT) to analyze the structure and chemistry of the near-apex regions of uncoated AFM tips as well as tips coated with a thin film of known composition. Atom probe tomography (APT) is a technique capable of concurrently determining three dimensional material structure and chemistry at near atomic resolution which has seen expanding use in science and engineering fields (Cojocaru-Miredin, et al., 2009; Danoix & Auger, 2000; Gopalan, et al., 2004; Gorman, et al., 2006; Hono, 2002; Hono & Ping, 2000; Kelly, et al., 2007; Kelly & Miller, 2007; Larson, et al., 1999; Perea, et al., 2008; Seidman, 2007; Thompson, et al., 2006).

2.3 Atom Probe Tomography

APT works on the phenomena of field evaporation, by which surface atoms of the specimen are ionized in ultra high vacuum and subsequently desorbed by an electric field (Muller & Bahadur, 1956). A schematic of the APT instrumentation is shown in Figure 1. The field evaporation process is effectively controlled by utilizing a cryogenically cooled (to reduce atomistic vibrations) needle-shaped specimen (to increase the electric field magnitude for evaporation) that is kept at a standing voltage while a local electrode is given a

pulsed voltage. The sample is traditionally prepared into a sharp needle shape with a tip radius on the order of 100nm by electropolishing a wire sample or using a focused ion beam to mill a tip (Larson, et al., 2001; Miller, et al., 2005; Thompson, et al., 2004; Zhou, et al., 2001). The standing voltage on the sample is kept close to the voltage needed for field evaporation, and the pulsed voltage on the local electrode is used to increase the field just enough to allow one atom to field evaporate. The ionized atom is then repelled through a hole in the local electrode towards a wide-angle position-sensitive detector equipped with a time-of flight mass spectrometer with single atom sensitivity. Typical magnifications of the specimen at the detector in most APT instruments are about 5-6 million times. The lateral coordinates of the ions are calculated from the recorded impact position on the detector, whereas the depth coordinate along the specimen axis is calculated from the ion position in the evaporation sequence (Bas, et al., 1995; Miller, 2000; Miller & Russell, 2007). Finally, the spatial coordinates of each atom are combined with its elemental identity from the time of flight data to create a 3D computer reconstruction of the analyzed region of the sample. Spatial resolution is limited by small trajectory aberrations of the ions close to the specimen surface and is typically ~0.2 nm laterally and ~0.05 nm in the depth coordinate (Miller, 2001). Detailed descriptions of the physical principle and performance of the method can be found in various books and review articles (Bas, et al., 1995; Kelly, et al., 2007; Kelly & Miller, 2007; Miller, 2000; Miller, 2001; Miller & Russell, 2007; Sanchez, et al., 2004). As a

comparison, energy filtering transmission electron microscopy (EFTEM) can provide two-dimensional chemical mapping with about 1 nm lateral resolution, which is limited by signal to noise issues (Grogger, et al., 2003). A direct comparison of identical calibration structures demonstrated that the spatial resolution of the local chemical analysis by APT exceeds that of the unprocessed EFTEM by a factor of 2 (Stender, et al., 2009). Thus APT is one of the highest resolution three dimensional nanoscale analysis tools presently available.

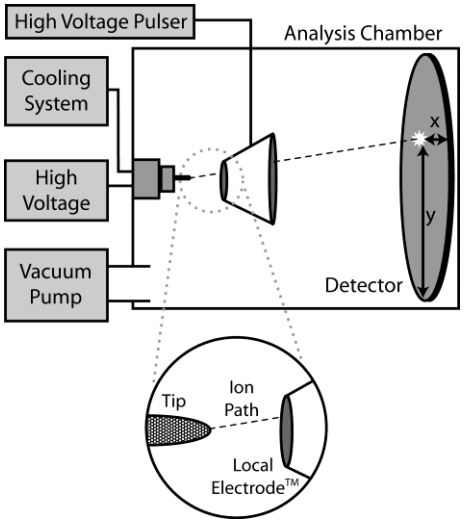

Figure 1. Diagram of an atom probe microscope. A short voltage pulse set up between the sample and the local electrode is used to ionize and remove an atom from the surface of the sample. It then passes through a hole in the local electrode to hit a position sensitive detector.

2.4 Materials and Methods

AFM tips are typically conical or pyramidal and have an apex radius ranging from tens of nanometers to microns depending on the type of investigation and the dimensions of the feature of interest. The similar tip geometry of AFM tips compared to a traditionally fabricated APT sample makes it a good candidate for APT.

In this study, two different commercially available AFM tips were studied - NSC15 (MikroMasch) and HAR5 (Nanoscience Instruments Inc.). While both the tips are made from silicon (Si) oriented along the (100) direction, the NSC15 has faceted sides and the HAR5 is smooth as shown in Figure 2. The HAR5 also has a larger aspect ratio (5:1 compared to 3:1 for NSC15) and the backside of the cantilever is coated with aluminum for reflectivity in AFM experiments. For comparison purposes, standard Si microtip specimens (fabricated array of sharp Si tips on a Si substrate available from IMAGO Scientific Instruments, Madison, WI) were also studied. The microtips provide consistent data and have been well studied (Thompson, et al., 2007). Both the AFM tips and the microtip specimens were mounted using a commercially available clip holder (IMAGO Scientific Instruments) to allow analysis of the AFM tips without the need for permanent mounting.

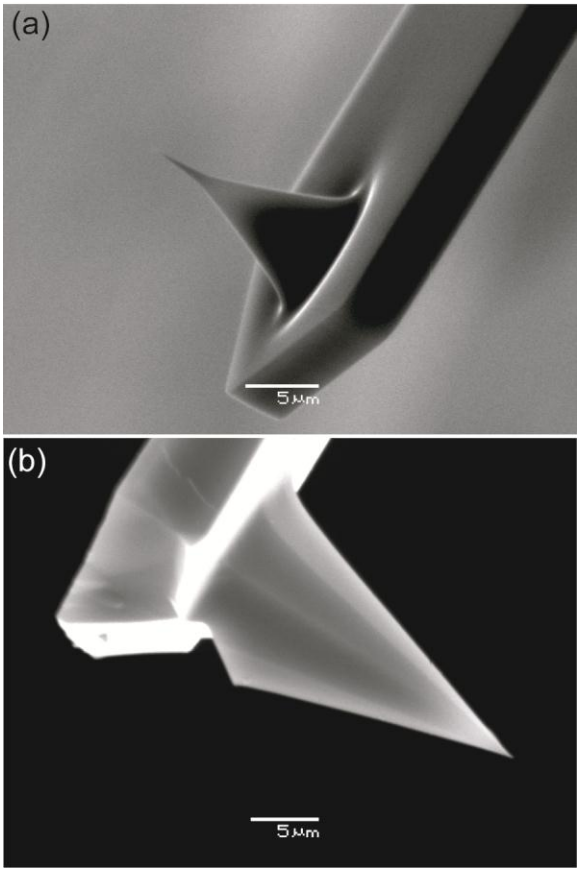

Figure 2. SEM images of the HAR5 (a) and NSC15 (b) AFM tips. The HAR5 tip has a larger aspect ratio and is not faceted.

In addition to uncoated tips, a NSC15 AFM tip and a microtip coupon were sputter deposited with a simple thin film with known composition to determine the ability to analyze a thin film on an AFM tip. Cu was chosen for the film primarily because of its similar evaporative field compared to Si. This reduces the stress when field evaporating through the interface. The tips were plasma cleaned for

30 seconds before depositing Cu for 2 minutes at 0.11nm/second to give an estimated film thickness of 13nm.

The samples were analyzed using a LEAP 3000x (IMAGO) atom probe microscope in voltage mode. Experiments were conducted at $4x10^{-11}$ Torr or less and the samples were cooled to at least 75K. All data was collected in a pulsed voltage mode at 200 kHz, using a 15% pulse fraction, and a 160mm flight path. The approximate measured volume for the reconstructions presented here are 30nmx30nmx10nm for uncoated samples and 30nmx30nmx80nm for coated samples.

We note that radii of the AFM tips were obtained experimentally by reverse imaging a sharp tip characterizer sample (TGT-1, NT-MDT) in a Dimension 3100 AFM (Veeco Instruments, Santa Barbara, CA) and reconstructing the tip shape using established methods (Bykov, et al., 1998; Villarrubia, 1997; Williams, et al., 1996). The tip radius is one of the parameters used in the software-based reconstruction of the atom positions in APT. Consequently the ability to determine a priori, a relatively accurate tip radius helps minimize errors in the reconstruction (Miller, 2000). The tip radii for the AFM tips in this study were on the order of tens of nanometers. Figure 3 shows the tip profile of the HAR 5 tip that was used to obtain the data shown in Figure 4b.

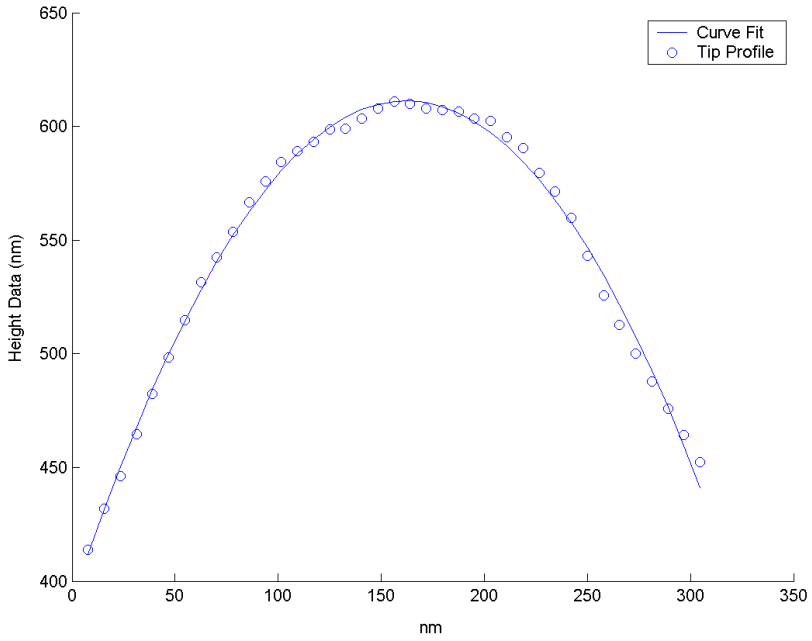

Figure 3. AFM tip profile obtained using a tip characterization sample. The curve fit was used to calculate a tip radius.

2.5 Results and Discussion

The first 10 nanometers of the reconstructions of uncoated AFM tips and microtip are shown in Figure 4. The data shows dark regions caused by local trajectory aberrations in the field evaporation of the Si atoms around the <100> pole, confirming that both AFM tip types and the microtips are composed of Si orientated along the <100> direction (Vurpillot, et al., 1999). The data lends confidence to the feasibility of analyzing AFM tips using APT.

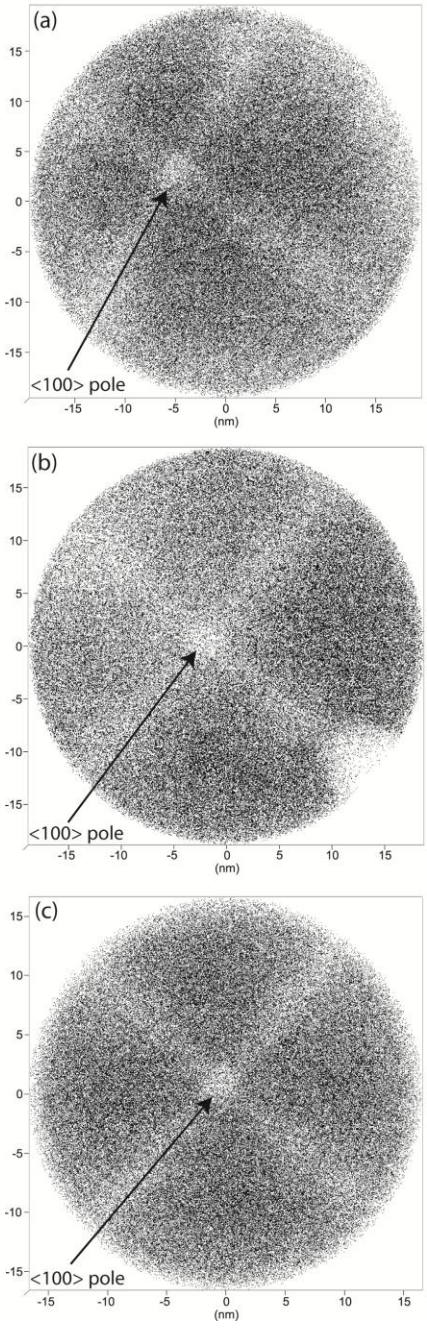

Figure 4. The first 10 nm of the NSC15 (a), HAR5 (b), and microtip (c) reconstructions looking down the analysis direction, all dimensions in nm. The Si <100> pole is highlighted.

A TEM analysis of the Cu coated NSC15 tip yielded a film thickness estimate of 11 nm as shown in Figure 5. Figures 6 and 7 show a slice through the APT data for a coated NSC15 tip and microtip respectively. The slices display only a percentage of the atoms for visual clarity. The Cu layer and the Si bulk can be easily discerned, and the inset in each figure shows a magnified view that highlights the interface. The estimated film thickness from the APT data on the NSC15 and the microtip were 11nm and 10nm respectively, which agree very well with the expected film thickness from the TEM observation.

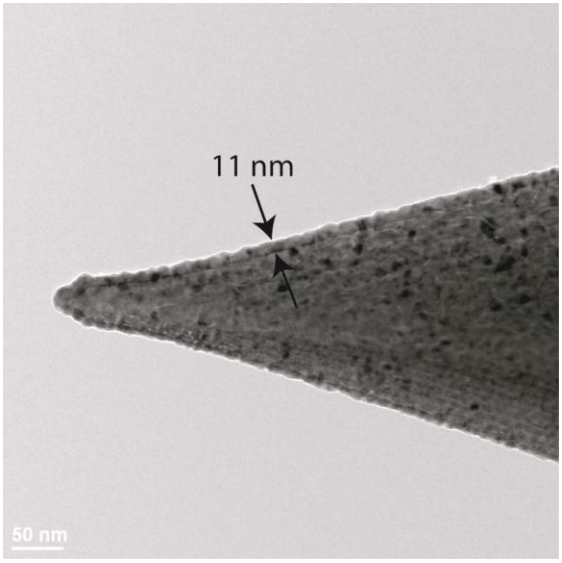

Figure 5. TEM image of a NSC15 AFM tip coated with Cu. The film thickness is highlighted.

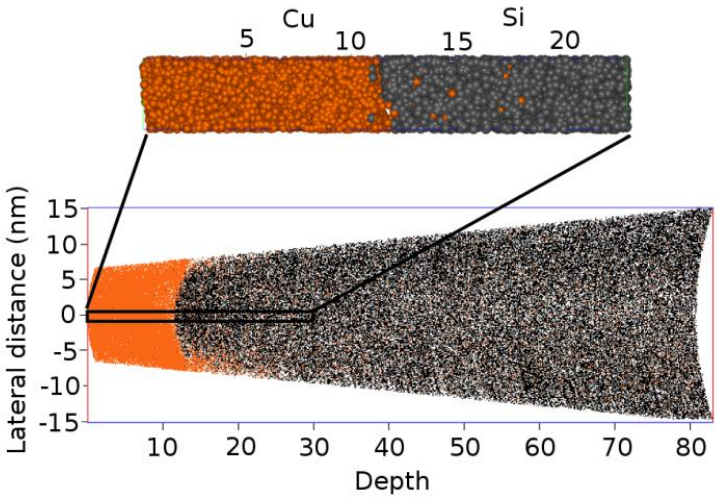

Figure 6. A slice of the reconstruction of a NSC15 tip sputter deposited with Cu with a blowup of the center of the analysis to show the Cu film thickness, dimensions in nm.

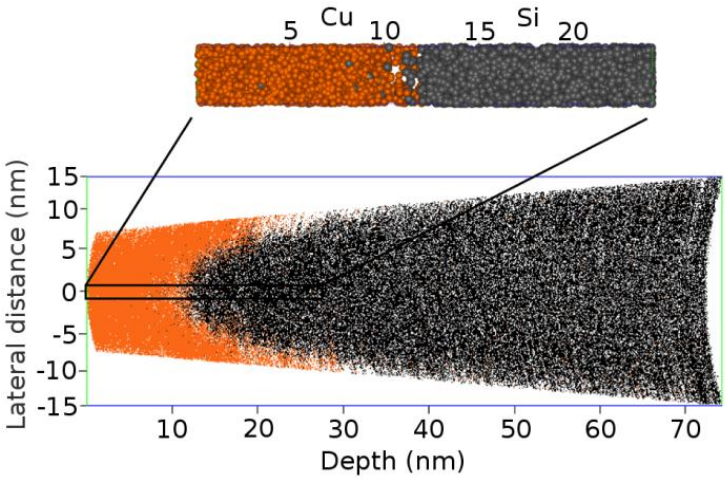

Figure 7. A slice of the reconstruction of a microtip sputter deposited with Cu with a blowup of the center of the analysis to show the Cu film thickness, dimensions in nm.

We note that the AFM cantilevers are free to bend when mounted on the clip holder in the atom probe microscope, and the electric field present in APT creates a force on the tip being analyzed (Mayama, et al., 2007). This force causes the AFM cantilever to bend during analysis which can affect the reconstruction since the tip axis will no longer be perfectly aligned with the local electrode axis during the field evaporative process. In preliminary tests with soft cantilevers (spring constants around 1N/m) it was seen that the bending could cause the tip to contact the local electrode and hence we moved to stiffer cantilevers. Simple finite element modeling in which a constant electrostatic field was assumed suggested that for the cantilevers used here (calibrated (Sader, et al., 1999) normal stiffness of 25N/m), the cantilever bending resulted in less than 5 degrees axis misalignment between the tip and the local electrode in the voltage range used for the experiments. A simple uncertainty (error) estimate in the reconstructed position of an atom caused by a sample tilt of this order was found to be about 9 Å for the lateral dimension and about 2 Å for the depth coordinate. We utilized the reconstruction method outlined by Bas et al. for our estimates. It is noted that this estimate is for a static deflection (for a given electric field) and a more detailed analysis on its affect on the APT data, especially in the real case of increasing field strength as the experiment progresses, is warranted. Continuous cantilever bending during the experiment can therefore contribute to considerable error in atom position data. It is worth noting that if the APT analysis is only concerned with material chemistry such as

percent solute analysis then the spatial error is not of great concern, especially if enough data is collected for proper statistics (Miller, et al., 1996). In our study, these errors did not significantly affect the measured values of film thickness measured thickness.

2.6 Conclusions

APT analysis was completed on both uncoated and thin film coated AFM tips and the results indicate that APT is a viable technique to obtain near atom-scale information of material structure and chemistry of the near-apex regions of such tips. This opens up a new avenue of investigation for AFM-related research. Possible topics of investigation range from assessing the durability and verifying the structure of thin films and coatings on an AFM tip to characterizing the structure and chemistry of transferred or newly generated material on the tip. Critical factors in the experiments were stiffness of the cantilever and mounting of the AFM tip in the atom probe microscope. Cantilevers with normal stiffness of 25 N/m and above appear to be viable for APT analysis. Our current and future work is aimed at a more detailed assessment of the effect of cantilever bending on the reconstruction and the analysis of transfer films from AFM-based wear studies.

Acknowledgements:

Funding for this study was provided by a grant from the National Science Foundation (Grant no. 0932573). The authors would also like to thank Matthew Kramer, from Ames Laboratory, for assistance in TEM analysis.

References

BAS, P., BOSTEL, A., DECONIHOUT, B. & BLAVETTE, D. (1995). A GENERAL PROTOCOL FOR THE RECONSTRUCTION OF 3D ATOM-PROBE DATA. Applied Surface Science **87/88**, 298-304.

BERGER, R., BUTT, H.J., RETSCHKE, M.B. & WEBER, S.A.L. (2009). Electrical Modes in Scanning Probe Microscopy. Macromolecular Rapid Communications **30**(14), 1167-1178.

BHUSHAN, B., ISRAELACHVILI, J.N. & LANDMAN, U. (1995). NANOTRIBOLOGY - FRICTION, WEAR AND LUBRICATION AT THE ATOMIC-SCALE. Nature **374**(6523), 607-616.

BUTT, H.J., CAPPELLA, B. & KAPPL, M. (2005). Force measurements with the atomic force microscope: Technique, interpretation and applications. Surface Science Reports **59**(1-6), 1-152.

BYKOV, V., GOLOGANOV, A. & SHEVYAKOV, V. (1998). Test structure for SPM tip shape deconvolution. Applied Physics a-Materials Science & Processing **66**(5), 499-502.

CARPICK, R.W. & SALMERON, M. (1997). Scratching the surface: Fundamental investigations of tribology with atomic force microscopy. Chemical Reviews **97**(4), 1163-1194.

CHEUNG, C.L., HAFNER, J.H. & LIEBER, C.M. (2000). Carbon nanotube atomic force microscopy tips: Direct growth by chemical vapor deposition and application to high-resolution imaging. Proceedings of the National Academy of Sciences of the United States of America **97**(8), 3809-3813.

CHUNG, K.H. & KIM, D.E. (2007). Wear characteristics of diamond-coated atomic force microscope probe. Ultramicroscopy **108**(1), 1-10.

COJOCARU-MIREDIN, O., CADEL, E., VURPILLOT, F., MANGELINCK, D. & BLAVETTE, D. (2009). Three-dimensional atomic-scale imaging of boron clusters in implanted silicon. Scripta Materialia **60**(5), 285-288.

DANOIX, F. & AUGER, P. (2000). Atom probe studies of the Fe-Cr system and stainless steels aged at intermediate temperature: A review. Materials Characterization **44**(1-2), 177-201.

FUJISAWA, S. & KIZUKA, T. (2003). Lateral displacement of an AFM tip observed by in-situ TEM/AFM combined microscopy: The effect of the friction in AFM. Tribology Letters **15**(2), 163-168.

GEWIRTH, A.A. & NIECE, B.K. (1997). Electrochemical applications of in situ scanning probe microscopy. Chemical Reviews **97**(4), 1129-1162.

GIANCARLO, L.C. & FLYNN, G.W. (1998). Scanning tunneling and atomic force microscopy probes of self-assembled, physisorbed monolayers: Peeking at the peaks. Annual Review of Physical Chemistry **49**, 297-+.

GOPALAN, R., PING, D.H., HONO, K., HUANG, M.Q., SMITH, B.R., CHEN, Z. & MA, B.M. (2004). Microstructure and magnetic properties of melt-spun Sm(Co0.58Fe0.31Cu0.04Zr0.05B0.02)(z) ribbons. Journal of Applied Physics **95**(9), 4962-4967.

GORMAN, B.P., NORMAN, A.G. & YAN, Y. (2006). Atom probe analysis of III-V and Si-based semiconductor photovoltaic structures. In 2nd Australian Workshop on Atom Probe Tomography, pp. 493-502. Sydney, AUSTRALIA.

GREENE, M.E., KINSER, C.R., KRAMER, D.E., PINGREE, L.S.C. & HERSAM, M.C. (2004). Application of scanning probe microscopy to the characterization and fabrication of hybrid nanomaterials. Microscopy Research and Technique **64**(5-6), 415-434.

GROGGER, W., SCHAFFER, B., KRISHNAN, K.M. & HOFER, F. (2003). Energy-filtering TEM at high magnification: spatial resolution and detection limits. Ultramicroscopy **96**(3-4), 481-489.

GRUVERMAN, A. & KHOLKIN, A. (2006). Nanoscale ferroelectrics: processing, characterization and future trends. Reports on Progress in Physics **69**(8), 2443-2474.

HANSMA, H.G. & PIETRASANTA, L. (1998). Atomic force microscopy and other scanning probe microscopies. Current Opinion in Chemical Biology **2**(5), 579-584.

HARTMANN, U. (1999). Magnetic force microscopy. Annual Review of Materials Science **29**, 53-87.

HOLMBERG, K., RONKAINEN, H. & MATTHEWS, A. (2000). Tribology of thin coatings. Ceramics International **26**(7), 787-795.

HONO, K. (2002). Nanoscale microstructural analysis of metallic materials by atom probe field ion microscopy. Progress in Materials Science **47**(6), 621-729.

HONO, K. & PING, D.H. (2000). Atom probe studies of nanocrystallization of amorphous alloys. Materials Characterization **44**(1-2), 203-217.

HORBER, J.K.H. & MILES, M.J. (2003). Scanning probe evolution in biology. Science **302**(5647), 1002-1005.

KALININ, S.V., RODRIGUEZ, B.J., JESSE, S., KARAPETIAN, E., MIRMAN, B., ELISEEV, E.A. & MOROZOVSKA, A.N. (2007). Nanoscale electromechanics of ferroelectric and biological systems: A new dimension in scanning probe microscopy. Annual Review of Materials Research **37**, 189-238.

KARUPPIAH, K.S.K., BRUCK, A.L. & SUNDARARAJAN, S. (2009a). Evaluation of Friction Behavior and Its Contact-Area Dependence at the Micro- and Nano-Scales. Tribology Letters **36**(3), 259-267.

KARUPPIAH, K.S.K., ZHOU, Y.B., WOO, L.K. & SUNDARARAJAN, S. (2009b). Nanoscale Friction Switches: Friction Modulation of Monomolecular Assemblies Using External Electric Fields. Langmuir **25**(20), 12114-12119.

KELLY, T.F., LARSON, D.J., THOMPSON, K., ALVIS, R.L., BUNTON, J.H., OLSON, J.D. & GORMAN, B.P. (2007). Atom probe tomography of electronic materials. Annual Review of Materials Research **37**, 681-727.

KELLY, T.F. & MILLER, M.K. (2007). Invited review article: Atom probe tomography. Review of Scientific Instruments **78**(3), 20.

KRONIK, L. & SHAPIRA, Y. (1999). Surface photovoltage phenomena: theory, experiment, and applications. Surface Science Reports **37**(1-5), 1-206.

LARSON, D.J., MARTENS, R.L., KELLY, T.F., MILLER, M.K. & TABAT, N. (1999). Atom probe analysis of planar multilayer structures. In 44th Annual

Conference on Magnetism and Magnetic Materials, pp. 5989-5991. San Jose, California: Amer Inst Physics.

LARSON, D.J., WISSMAN, B.D., MARTENS, R.L., VIELLIEUX, R.J., KELLY, T.F., GRIBB, T.T., ERSKINE, H.F. & TABAT, N. (2001). Advances in atom probe specimen fabrication from planar multilayer thin film structures. Microscopy and Microanalysis **7**(1), 24-31.

LILLEHEI, P.T. & BOTTOMLEY, L.A. (2000). Scanning probe microscopy. Analytical Chemistry **72**(12), 189R-196R.

LOOS, J. (2005). The art of SPM: Scanning probe microscopy in materials science. Advanced Materials **17**(15), 1821-1833.

MAGONOV, S.N. & RENEKER, D.H. (1997). Characterization of polymer surfaces with atomic force microscopy. Annual Review of Materials Science **27**, 175-222.

MARTINEZ, J., YUZVINSKY, T.D., FENNIMORE, A.M., ZETTL, A., GARCIA, R. & BUSTAMANTE, C. (2005). Length control and sharpening of atomic force microscope carbon nanotube tips assisted by an electron beam. Nanotechnology **16**(11), 2493-2496.

MAYAMA, N., YAMASHITA, C., KAITO, T., NOJIMA, M. & OWARI, M. (2007). Stress of needle specimen on the three-dimensional atom probe (3DAP). In 6th

International Symposiium on Atomic Level Characterization for New Materials and Devices, pp. 1610-1613. Kanazawa, JAPAN.

MILLER, M.K. (2000). Atom Probe Tomography Analysis at the Atomic Level. New York: Kluwer Academic/Plenum Publishers.

MILLER, M.K. (2001). Interface analysis with the three-dimensional atom probe. Surface and Interface Analysis **31**(7), 593-598.

MILLER, M.K., CEREZO, A., HETHERINGTON, M.G. & SMITH, G.D.W. (1996). Atom Probe Field Ion Microscopy. Oxford: Oxford University Press.

MILLER, M.K. & RUSSELL, K.F. (2007). Performance of a local electrode atom probe. Surface and Interface Analysis **39**(2-3), 262-267.

MILLER, M.K., RUSSELL, K.F. & THOMPSON, G.B. (2005). Strategies for fabricating atom probe specimens with a dual beam FIB. Ultramicroscopy **102**(4), 287-298.

MULLER, D.J. & DUFRENE, Y.F. (2008). Atomic force microscopy as a multifunctional molecular toolbox in nanobiotechnology. Nature Nanotechnology **3**(5), 261-269.

MULLER, E.W. & BAHADUR, K. (1956). FIELD IONIZATION OF GASES AT A METAL SURFACE AND THE RESOLUTION OF THE FIELD ION MICROSCOPE. Physical Review **102**(3), 624-631.

NICHOLLS, M.A., DO, T., NORTON, P.R., KASRAI, M. & BANCROFT, G.M. (2005). Review of the lubrication of metallic surfaces by zinc dialkyl-dithlophosphates. Tribology International **38**(1), 15-39.

OESTERSCHULZE, E. (2001). Recent developments of probes for scanning probe microscopy. In Advances in Imaging and Electron Physics, Vol 118, pp. 129-206.

PEREA, D.E., WIJAYA, E., LENSCH-FALK, J.L., HEMESATH, E.R. & LAUHON, L.J. (2008). Tomographic analysis of dilute impurities in semiconductor nanostructures. Journal of Solid State Chemistry **181**(7), 1642-1649.

POGGI, M.A., GADSBY, E.D., BOTTOMLEY, L.A., KING, W.P., OROUDJEV, E. & HANSMA, H. (2004). Scanning probe microscopy. Analytical Chemistry **76**(12), 3429-3443.

SADER, J.E., CHON, J.W.M. & MULVANEY, P. (1999). Calibration of rectangular atomic force microscope cantilevers. Review of Scientific Instruments **70**(10), 3967-3969.

SAMORI, P. (2004). Scanning probe microscopies beyond imaging. Journal of Materials Chemistry **14**(9), 1353-1366.

SANCHEZ, C.G., LOZOVOI, A.Y. & ALAVI, A. (2004). Field-evaporation from first-principles. Molecular Physics **102**(9-10), 1045-1055.

SANTOS, N.C. & CASTANHO, M. (2004). An overview of the biophysical applications of atomic force microscopy. Biophysical Chemistry **107**(2), 133-149.

SEIDMAN, D.N. (2007). Three-dimensional atom-probe tomography: Advances and applications. Annual Review of Materials Research **37**, 127-158.

STENDER, P., HEIL, T., KOHL, H. & SCHMITZ, G. (2009). Quantitative comparison of energy-filtering transmission electron microscopy and atom probe tomography. Ultramicroscopy **109**(5), 612-618.

TANAKA, K., YOSHIMURA, M. & UEDA, K. (2009). High-Resolution Magnetic Force Microscopy Using Carbon Nanotube Probes Fabricated Directly by Microwave Plasma-Enhanced Chemical Vapor Deposition. Journal of Nanomaterials.

THOMPSON, G.B., MILLER, M.K. & FRASER, H.L. (2004). Some aspects of atom probe specimen preparation and analysis of thin film materials. Ultramicroscopy **100**(1-2), 25-34.

THOMPSON, K., LARSON, D.J., ULFIG, R.M., BUNTON, J.H. & KELLY, T.F. (2006). Analyzing Si-based structures in 3D with a laser-pulsed local electrode atom probe. Solid State Technology **49**(6), 65-+.

THOMPSON, K., SEBASTIAN, J. & GERSTL, S. (2007). Observations of Si field evaporation. Ultramicroscopy **107**(2-3), 124-130.

VILLARRUBIA, J.S. (1997). Algorithms for scanned probe microscope image simulation, surface reconstruction, and tip estimation. Journal of Research of the National Institute of Standards and Technology **102**(4), 425-454.

VURPILLOT, F., BOSTEL, A., MENAND, A. & BLAVETTE, D. (1999). Trajectories of field emitted ions in 3D atom-probe. European Physical Journal-Applied Physics **6**(2), 217-221.

WADE, L.A., SHAPIRO, I.R., MA, Z.Y., QUAKE, S.R. & COLLIER, C.P. (2004). Correlating AFM probe morphology to image resolution for single-wall carbon nanotube tips. Nano Letters **4**(4), 725-731.

WILLIAMS, P.M., SHAKESHEFF, K.M., DAVIES, M.C., JACKSON, D.E., ROBERTS, C.J. & TENDLER, S.J.B. (1996). Blind reconstruction of scanning probe image data. Journal of Vacuum Science and Technology B **14**(2), 1557-1562.

WOUTERS, D. & SCHUBERT, U.S. (2004). Nanolithography and nanochemistry: Probe-related patterning techniques and chemical modification for nanometer-sized devices. Angewandte Chemie-International Edition **43**(19), 2480-2495.

XIE, X.N., CHUNG, H.J., SOW, C.H. & WEE, A.T.S. (2006). Nanoscale materials patterning and engineering by atomic force microscopy nanolithography. Materials Science & Engineering R-Reports **54**(1-2), 1-48.

ZHOU, X.W., WADLEY, H.N.G., JOHNSON, R.A., LARSON, D.J., TABAT, N., CEREZO, A., PETFORD-LONG, A.K., SMITH, G.D.W., CLIFTON, P.H., MARTENS, R.L. & KELLY, T.F. (2001). Atomic scale structure of sputtered metal multilayers. Acta Materialia **49**(19), 4005-4015.

CHAPTER 3. DETECTION AND ANALYSIS OF THE NATIVE OXIDE LAYER ON THE NEAR APEX REGION OF ATOMIC FORCE MICROSCOPE TIPS USING LASER PULSED ATOM PROBE TOMOGRAPHY

Modified from a paper submitted to Microscopy and Microanalysis

Christopher J. Tourek, Sriram Sundararajan

3.1 Abstract

In atomic force microscopy (AFM), it is well recognized that the surface layers on the tip and sample greatly affect the tip-sample interactions and the resulting measurements. One important question pertaining to silicon tips is the presence and thickness of the surface native oxide layer at the near-apex region of the tip. In this study, we have used the atomic scale characterization capabilities of atom probe tomography (APT) to investigate the structure and chemistry of the near-apex region of three types of commercial dry and wet etched silicon AFM tips. The results show that a native oxide layer is present on all three types of tips with thicknesses ranging from 0.5-1.5nm. The tips also show the presence of water molecules and in one type, the presence of aluminum, which is used as a reflective coating on the cantilever backside. The oxide species are shown to be readily detected using APT in the laser pulsed

mode as opposed to voltage pulsed mode. Consequently analysis of AFM tips using APT in laser pulsed mode can expand the capabilities of SPM-based interrogation of surface and interfacial phenomena.

3.2 Introduction

Over the past 25 years, atomic force microscopy (AFM), or more generally, scanning probe microscopy (SPM), has become one of the most powerful tools in the fields of nanoscience and nanotechnology for the preparation and analysis of materials, nanostructures and their functionality (Bhushan, et al., 1995; Carpick & Salmeron, 1997; Lillehei & Bottomley, 2000; Loos, 2005). Over the years, the basic principle of AFM/SPM – measuring a specific interaction between an ultra-sharp tip and a material's surface to collect structural or functional information, has generated a whole range of techniques such as friction force microscopy, electrical force microscopy, magnetic force microscopy and scanning probe lithography, to name a few. Using specific tips and measuring conditions, a whole range of data can be measured (Butt, et al., 2005; Giancarlo & Flynn, 1998; Muller & Dufrene, 2008; Samori, 2004). SPM based techniques have especially been useful in the field of nanotribology, the study of friction, adhesion, lubrication and wear at contacts of nanometer sizes (Bhushan, 1998; Bhushan, et al., 1995; Carpick & Salmeron, 1997; Szlufarska, et al., 2008).

Obtaining a fundamental understanding of these phenomena requires careful experiments at well-defined forces and surfaces. The use of probe shape characterizers and reconstruction algorithms allow precise evaluation and monitoring of the tip shape during experiments. Techniques to reliably calibrate the normal and lateral spring constants of the cantilevers allow researchers to perform more accurate force measurements (Torii, et al., 1996), and calibration methods to perform quantitative friction force microscopy are available (Ogletree, et al., 1996; Ruan & Bhushan, 1994). It is well recognized that the surface layers on the tip and sample surface greatly affect the tip-sample interactions and AFM-related measurements. Consequently, a detailed assessment of the material structure and chemistry of the near apex region of the scanning probe or AFM tip can provide further insights into the observed phenomena. Specific areas that would directly benefit from this information include fabrication and friction/wear studies using AFM tips where material transfer and tip chemistry are of importance (Chung & Kim, 2007; Karuppiah, et al., 2009a; Karuppiah, et al., 2009b). Few techniques exist that can provide this critical information because of the small size of the AFM tips. Researchers have attempted to quantify contamination on the chip and cantilevers, and these studies assumed that the surface species detected in these regions would also exist at the apex of the tip (Bonaccurso & Gillies, 2004; Lo, et al., 1999; Sirghi, et al., 2006). Work has also been done to combine SPM with time of flight mass spectrometry (Lee, et al., 2004; Wetzel, et al., 2005) to assess the chemistry of the tip in-situ; however

these time of flight studies describe vacuum conditions and the 3D structure of the atomic positions could not be obtained with this technique. More recently, we utilized three dimensional atom probe tomography (APT) to successfully interrogate the material structure and chemistry of the near apex regions of commercial AFM tips to the near atomic-scale (Tourek & Sundararajan, 2009).

APT is a technique capable of concurrently determining three dimensional material structure and chemistry at near atomic resolution which has seen expanding use in science and engineering fields (Kelly & Miller, 2007; Seidman, 2007; Thompson, et al., 2006). APT works on the phenomenon of field evaporation, by which surface atoms of the specimen are ionized in ultra high vacuum and subsequently desorbed by an electric field (Muller & Bahadur, 1956). A schematic of the APT instrumentation is shown in Figure 1. The field evaporation process is controlled by utilizing a cryogenically cooled (to reduce atomistic vibrations) needle-shaped specimen (to increase the electric field magnitude) in an electric field. The sample is traditionally prepared into a sharp needle shape with a tip radius on the order of 10's of nm by electropolishing a wire sample or using a focused ion beam to mill a tip (Miller, et al., 2005; Thompson, et al., 2004). A standing voltage is applied to the sample and kept close to the voltage needed for field evaporation. Then a voltage pulse to a local electrode or laser pulse to the sample is used to excite one atom to field evaporate. The ionized atom is repelled by the electric field through a hole in the local electrode towards a wide-angle position-sensitive detector equipped with a

time-of flight mass spectrometer with single atom sensitivity. Typical magnifications of the specimen at the detector in most APT instruments are about 5-6 million times. The lateral coordinates of the ions are calculated from the recorded impact position on the detector, and the depth coordinate along the specimen axis is calculated from the ion position in the evaporation sequence (Bas, et al., 1995; Miller, 2000; Miller & Russell, 2007). Finally, the spatial coordinates of each atom are combined with its elemental identity from time of flight data to create a 3D computer reconstruction of the analyzed region of the sample. Spatial resolution is limited by small trajectory aberrations of the ions close to the specimen surface and is typically ~0.2 nm laterally and ~0.05 nm in the depth coordinate (Miller, 2001). Detailed descriptions of the physical principle and performance of the method can be found in various books and review articles (Kelly & Miller, 2007; Miller, 2000). As a comparison, energy filtering transmission electron microscopy (EFTEM) can provide two-dimensional chemical mapping with about 1 nm lateral resolution, which is limited by signal to noise issues (Grogger, et al., 2003). A direct comparison of identical calibration structures demonstrated that the spatial resolution of the local chemical analysis by APT exceeds that of the unprocessed EFTEM by a factor of 2 (Stender, et al., 2009). Thus APT is one of the highest resolution three dimensional nanoscale analysis tools presently available.

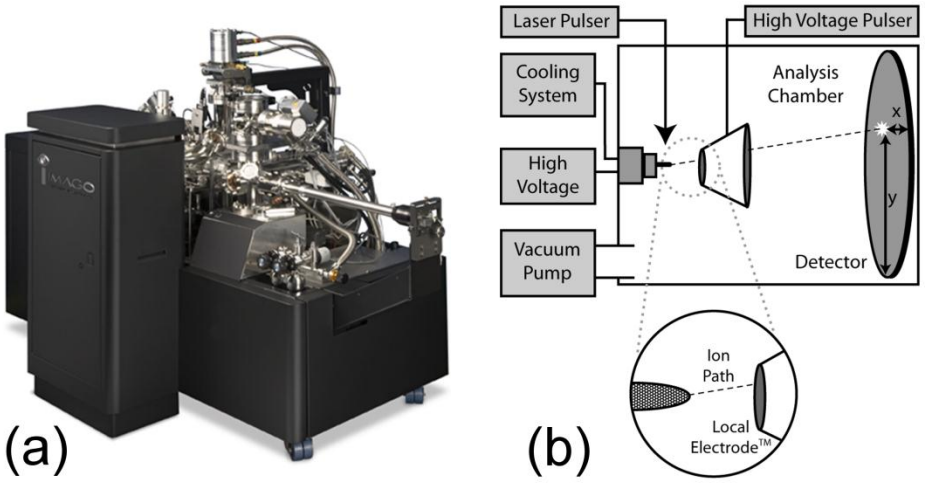

Figure 1. A commercial atom probe microscope (LEAP 3000X Si) and a schematic of the key elements associated in an atom probe microscope.

Commercial AFM tips are available having a conical tip with a tip radius less than 100nm which is a geometry that is suitable for analysis by APT. By utilizing an appropriate holder an AFM tip can be successfully examined using APT and 3D reconstructions of the atom positions in the near apex region of the AFM tip can be obtained, as demonstrated in our previous work (Tourek & Sundararajan, 2009). Most commercially available Si tips are expected to have a native oxide layer, and while studies have provided oxide layer thicknesses from flat samples (Cotirlan, et al., 2010; Negrila, et al., 2008; Tomizuka & Ayame, 1995), to our knowledge the oxide layer at the near apex region of the AFM tip remains un-investigated. In this paper we report on our investigations using APT to quantify

the native oxide layer present at the near apex region of commercially available Si AFM tips.

3.3 Methods and Materials

Three different commercially available tips were investigated, HAR5 (Team Nanotec available through Nanoscience Instruments, Inc.), Aspire CT300 (Nanoscience Instruments, Inc.) and NSC15 (MikroMasch). Both the HAR5 and Aspire types are dry etched conical where as the NSC15 tips are wet etched and slightly pyramidal with faceted sides. All three tips are orientated along the Si (100) direction and are n-type with antimony doping in the HAR5 and Aspire tips and phosphorus doping in the NSC15 tips. Scanning electron micrographs of typical HAR5, Aspire and NSC15 tips used in the study are shown in Figure 2 (a-c). An important factor in successful APT experiments is for the sample to have a smooth tip with a reasonably well-defined radius. Also *a priori* knowledge of the tip radius helps minimize errors in the reconstruction as the radius is one of the parameters used in the software-based reconstruction of the atom positions in APT (Miller, 2000). Consequently the tip radius of each brand new AFM tip was obtained prior to APT analysis by reverse imaging (Bykov, et al., 1998; Villarrubia, 1997; Williams, et al., 1996) the tip in intermittent contact mode using a silicon tip characterizer (TGT1, NT-MDT) on a Dimension 3100 AFM (Nanoscope IV, Veeco Instruments). Figure 2 (d) shows a typical AFM tip profile

along with the approximate volume that is typically analyzed and reconstructed in APT measurements. Tip radii of all three AFM tip types are typically less than 30nm.

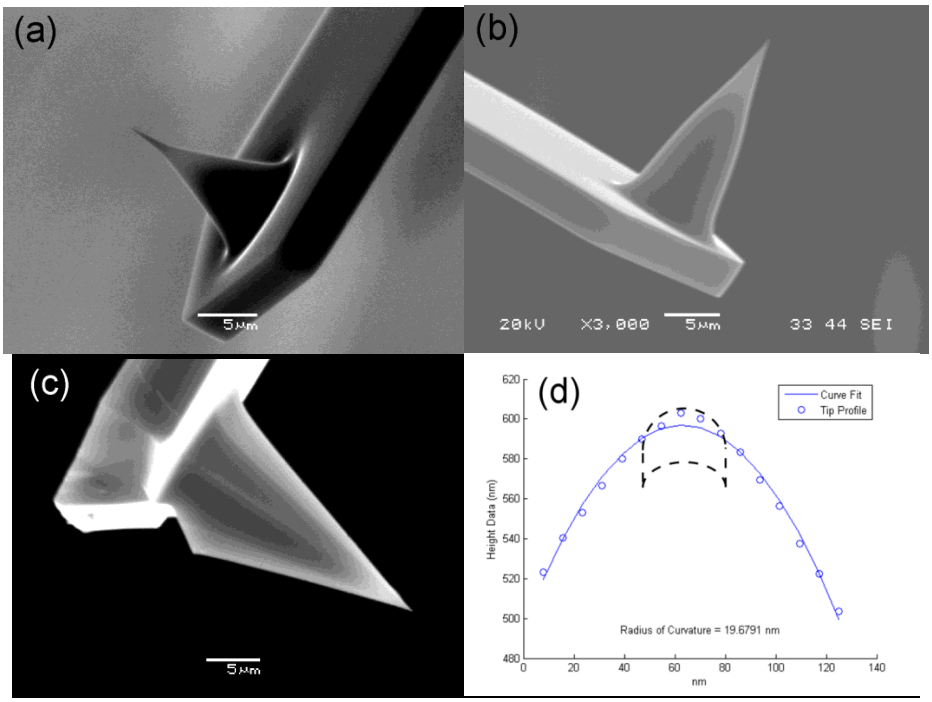

Figure 2. SEM image of a typical commercial Si (100) HAR5 (a) Aspire (b) and NSC15 (c) AFM tips used in the experiments and an example of a tip profile (d) obtained via scanning a tip characterizer in an AFM to determine the radius. The dashed box highlights the approximate region of APT analysis.

The tips were subsequently analyzed using a commercially available atom probe microscope (LEAP 3000X Si, Cameca Instruments Inc.) in laser pulsed mode. Laser pulsed mode is typically utilized for low electrically conductive specimens, including oxides. After obtaining the tip radius, the AFM tips were loaded into the atom probe microscope using a clip holder (Cameca Instruments Inc.), which allowed analysis of the AFM tip without the need for permanent mounting. Typically in APT an initial visual alignment of the sample is done with respect to the local electrode before turning on the bias, then a finer alignment is conducted while detecting ions from the sample. Since we are trying to detect ions at the surface, it is preferable to minimize alignment after detection has started to minimize any loss. To address this issue, a silicon microtip sample (Cameca Instruments Inc.) with similar geometry and doping to the AFM tips was used to align and focus the laser system prior to the AFM run. Then the microtip was exchanged for the AFM tip without moving the laser position and the AFM tip was brought into alignment with the laser, placing it in proper alignment with the local electrode. Experiments were conducted at $2x10^{-11}$ Torr or less, 60 K or less, 200 kHz, and a 160 mm flight path. A 0.3nJ laser pulse was used for the laser power because it produces reliable data for the microtip sample. Reconstruction of the APT runs was done using IVAS software (Cameca Instruments Inc.) utilizing the experimentally determined tip radius.

3.4 Results and Discussion

Typical mass spectra from APT analysis for a HAR5, Aspire, and NSC15 AFM tip are shown in Figure 3. All spectra were obtained from about 90,000 atom at the beginning of the run. Not only were Si+ (28 Da main peak), Si++ (14), O+ (16) and SiO_2+ (60) indicative of an oxide detected, but also O_2+ (32) Si_2+ (56) SiO+ (44) SiO++ (22) Si_2O+ (72) and Si_2O++ (36) which is consistent with the near interface region of the oxide (Cotirlan, et al., 2010; Himpsel, et al., 1988). It is noted that Si_2++ (28) and SiO_2++ (30) overlap with the isotopes of Si+ in the mass spectrum and therefore are not readily visible. H_2O+ (28) is also visible in the mass spectrum and could be a surface contaminant on the tip. Organic contaminants of the type reported by Sirghi et al (Sirghi, et al., 2006) on the cantilevers of AFM tips were not seen by APT on the tip apex. Either these physisorbed contaminants are negligible at the tip apex or they may have out gassed in the ultra-high vacuum used in APT. However on the NSC15 tips the mass spectra show presence of C+ (12), F+ (19) and C2F+ (43) which is indicative of CF chains as contamination. Also all the NSC15 spectra show the presence of Al on the tip apex, which most likely arose from the deposition of Al on the back of the cantilever. Al coatings are typically used to improve reflectivity of the laser light off of the cantilever for AFM experiments. We note that while the NCS15 showed the presence of Al, the two other tip types, which also have Al coatings on the cantilever backside, did not.

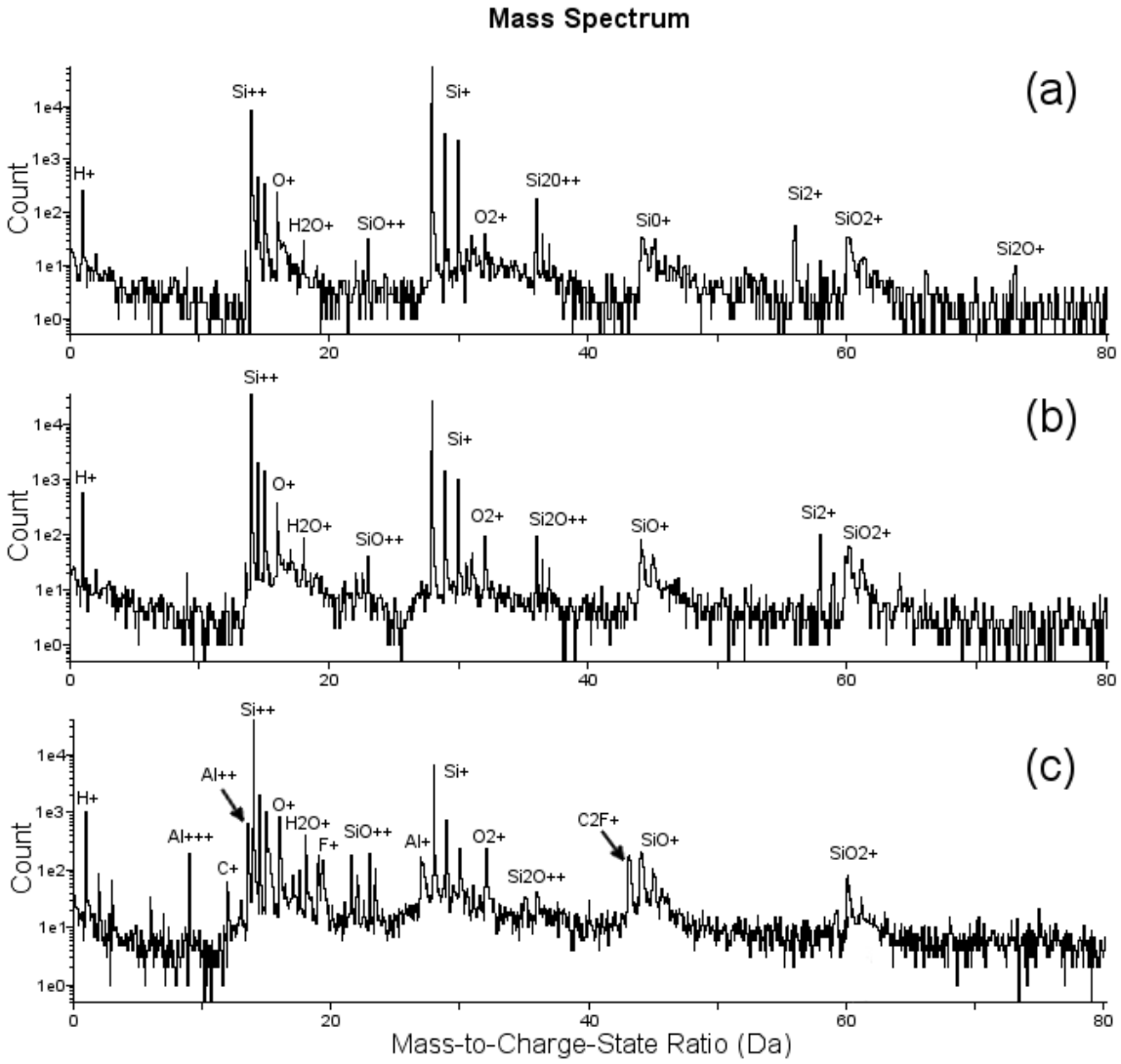

Figure 3. Mass spectra of a HAR5 (a) Aspire (b) and NSC15 (c) AFM tip analysed by APT. All spectra contain about 90,000 atoms and show that the oxides are readily analyzed in laser pulsed mode for the tips.

A 5nm cube of the APT reconstruction of a HAR5, Aspire, and NSC15 AFM tip are shown in Figure 4. The cubes are taken from the center of the reconstruction at the surface, and show that the oxide species reside mostly at the surface and extend only a few atomic layers, strongly indicative of a surface layer. 5 HAR5 tips, 4 Aspire tips, and 3 NSC15 tips were analyzed by APT, and all tips showed oxides in the mass spectrum. An analysis of 1-D concentration profiles normal to the surface from the reconstructions revealed the constant concentration region of the oxide on the HAR5 tip to be about 0.6nm with an intermixing zone of about 1nm. These values for the Aspire tips were 0.7 and 0.3 nm while for the NSC15 tips they were 1.5 and 0.5 nm respectively. The NSC15 tips consistently showed a significantly thicker oxide layer than the other tips which may be due to the difference in manufacturing techniques. The thickness values agree well with estimations of the native oxide layer on (100) Si given in the literature, which are 0.5 - 1.5 nm depending on exposure length to air (Cotirlan, et al., 2010; Negrila, et al., 2008; Tomizuka & Ayame, 1995).

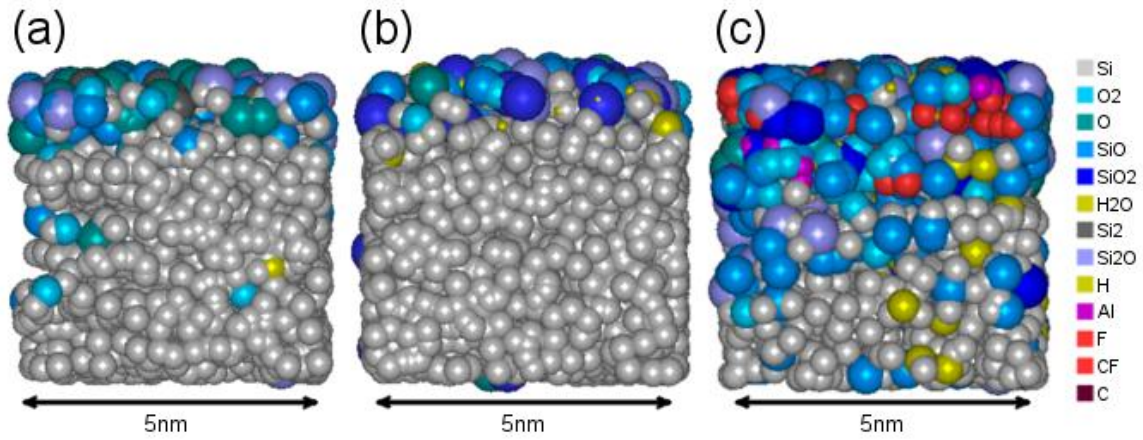

Figure 4. A small region of the APT reconstruction of a typical HAR5 (a), Aspire AFM tip (b) and NSC15 (c). Each sphere represents an ion location and the color represents the species. The reconstructions are a 5nm cube from the surface at the center of the reconstruction that highlights the thickness of the native oxide layer on the AFM tip.

It is worth noting that our previous work in voltage pulsed mode (Tourek & Sundararajan, 2009) did not detect an oxide layer on HAR5 tips. As shown in the current study, the oxide layer is readily detectable using laser pulsed mode. Figure 5 shows a series of mass spectra from 3 APT experiments performed on the same HAR5 tip in succession. The first and third experiment were done in laser pulsed mode and the second experiment was done in voltage pulsed mode. All three experiments were done in succession without moving the tip with about 250,000 ions detected in each run. The oxide species on the tip are readily seen in the laser pulsed mode experiments, but are absent in the voltage mode

experiment. The curvature of the sample and an off center alignment allowed the oxide layer to be in the analysis volume throughout all three experiments. This ability to detect oxides more readily in laser pulsed mode has also been noted for other materials (Ito, et al., 2008; Seidman, 2007) and while it is still unclear as to the specific reasons for this observation, the observations have been attributed to the lower electrical conductivity of the oxides as well as oxygen species evaporating in between the voltage pulses (Seidman, 2007). This experiment nevertheless highlights the advantage of using laser pulsed APT to analyze surface layers in AFM tips, especially where non-conductive materials may be present.

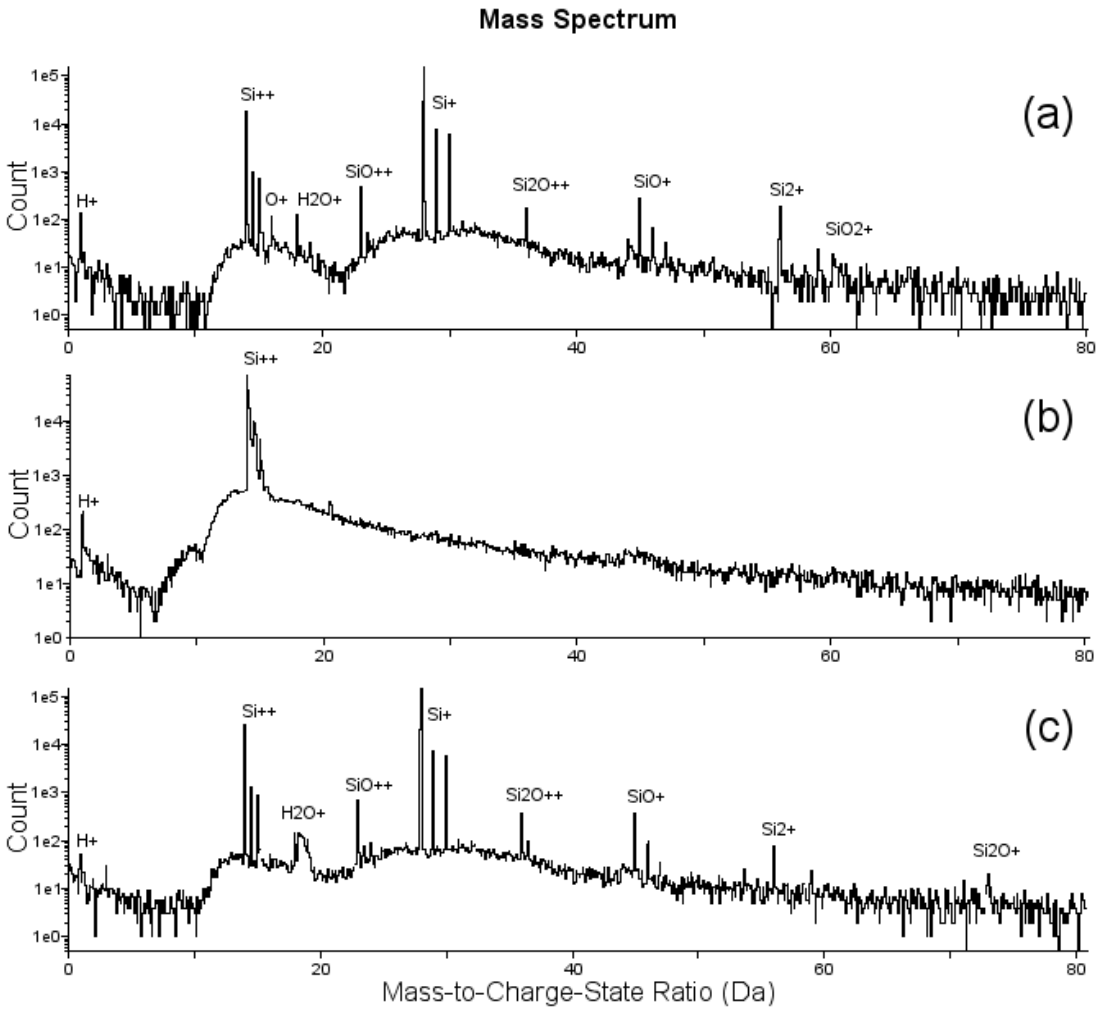

Figure 5. Mass spectra from successive runs on a single HAR5 tip, each run consisting of 250,000 atoms. The first mass spectrum (a) shows a laser pulsed mode run, the second spectrum (b) shows a voltage pulsed run, and the third (c) shows a laser pulsed run. All three runs were done on the same tip in succession without moving the sample. The comparison shows oxides are readily analyzed in laser pulsed mode, but not in voltage pulsed mode.

3.5 Conclusions

In this study, we have utilized APT in laser pulsed mode to evaluate the structure and chemistry of the near-apex region of AFM tips at the near-atomic scale. In particular we have been able to provide a direct assessment of the native oxide layer in three types of commercially available dry-etched Si tips. A native oxide layer of a 0.5, 0.7, and 1.5nm on HAR5, Aspire, and NSC15 AFM tips respectively was readily detected. In addition the NSC15 tips showed aluminum likely from the backside coating process. The oxide species on the tips are shown to be readily detected using APT in laser pulsed mode but not in voltage pulsed mode. Consequently APT in laser pulsed mode is a powerful analytical tool that can expand the capabilities of SPM-based interrogation of surface and interfacial phenomena by allowing direct investigation of surface layers on the near-apex regions of AFM tips. For example, it can be a useful technique to access the applicability of AFM tips for an experiment by investigating the chemical composition and structure of any contaminates along with the thickness of the native oxide layer.

Acknowledgments

Partial funding for this study was provided by grants from the National Science Foundation (Grant no. CBET 0932573) and the W.M. Keck Foundation.

The authors would also like to thank Joseph Grech at Nanoscience Instruments and Jamie Arnold at MikroMasch for help in acquiring details on the AFM probes.

References

Bas, P., Bostel, A., Deconihout, B. & Blavette, D. (1995). A GENERAL PROTOCOL FOR THE RECONSTRUCTION OF 3D ATOM-PROBE DATA. Applied Surface Science 87/88, 298-304.

Bhushan. (1998). Handbook of Micro/Nanotribology Second Edition.

Bhushan, B., Israelachvili, J.N. & Landman, U. (1995). NANOTRIBOLOGY - FRICTION, WEAR AND LUBRICATION AT THE ATOMIC-SCALE. Nature 374(6523), 607-616.

Bonaccurso, E. & Gillies, G. (2004). Revealing contamination on AFM cantilevers by microdrops and microbubbles. Langmuir 20(26), 11824-11827.

Butt, H.J., Cappella, B. & Kappl, M. (2005). Force measurements with the atomic force microscope: Technique, interpretation and applications. Surface Science Reports 59(1-6), 1-152.

Bykov, V., Gologanov, A. & Shevyakov, V. (1998). Test structure for SPM tip shape deconvolution. Appl. Phys. A-Mater. Sci. Process. 66(5), 499-502.

Carpick, R.W. & Salmeron, M. (1997). Scratching the surface: Fundamental investigations of tribology with atomic force microscopy. Chemical Reviews 97(4), 1163-1194.

Chung, K.H. & Kim, D.E. (2007). Wear characteristics of diamond-coated atomic force microscope probe. Ultramicroscopy 108(1), 1-10.

Cotirlan, C., Galca, A.C., Ciobanu, C.S. & Logofatu, C. (2010). The study of the silicon oxide thickness on crystalline Si by X-ray photoelectron spectroscopy and spectroscopic ellipsometry. J. Optoelectron. Adv. Mater. 12(5), 1092-1097.

Giancarlo, L.C. & Flynn, G.W. (1998). Scanning tunneling and atomic force microscopy probes of self-assembled, physisorbed monolayers: Peeking at the peaks. Annual Review of Physical Chemistry 49, 297-+.

Greenwood, N.N. & Earnshaw, A. (1997). Chemistry of the Elements. pp. 1344p.: Elsevier.

Grogger, W., Schaffer, B., Krishnan, K.M. & Hofer, F. (2003). Energy-filtering TEM at high magnification: spatial resolution and detection limits. Ultramicroscopy 96(3-4), 481-489.

Himpsel, F.J., McFeely, F.R., Taleb-Ibrahimi, A., Yarmoff, J.A. & Hollinger, G. (1988). Microscopic structure of the SiO2/Si interface. Physical Review B 38(9), 6084.

Ito, S., Kaneko, T., Yamashita, C., Kaito, T., Adachi, T., Iwata, T., Mayama, N., Nojima, M., Taniguchi, M. & Owari, M. (2008). Development of preset-type sample stage in three-dimensional atom probe. Surface and Interface Analysis 40(13), 1696-1700.

Karuppiah, K.S.K., Bruck, A.L. & Sundararajan, S. (2009a). Evaluation of Friction Behavior and Its Contact-Area Dependence at the Micro- and Nano-Scales. Tribology Letters 36(3), 259-267.

Karuppiah, K.S.K., Zhou, Y.B., Woo, L.K. & Sundararajan, S. (2009b). Nanoscale Friction Switches: Friction Modulation of Monomolecular Assemblies Using External Electric Fields. Langmuir 25(20), 12114-12119.

Kelly, T.F. & Miller, M.K. (2007). Invited review article: Atom probe tomography. Review of Scientific Instruments 78(3), 20.

Lee, D., Wetzel, A., Bennewitz, R., Meyer, E., Despont, M., Vettiger, P. & Gerber, C. (2004). Switchable cantilever for a time-of-flight scanning force microscope. Applied Physics Letters 84(9), 1558-1560.

Lillehei, P.T. & Bottomley, L.A. (2000). Scanning probe microscopy. Analytical Chemistry 72(12), 189R-196R.

Lo, Y.S., Huefner, N.D., Chan, W.S., Dryden, P., Hagenhoff, B. & Beebe, T.P. (1999). Organic and inorganic contamination on commercial AFM cantilevers. Langmuir 15(19), 6522-6526.

Loos, J. (2005). The art of SPM: Scanning probe microscopy in materials science. Advanced Materials 17(15), 1821-1833.

Miller, M.K. (2000). Atom Probe Tomography Analysis at the Atomic Level. New York: Kluwer Academic/Plenum Publishers.

Miller, M.K. (2001). Interface analysis with the three-dimensional atom probe. Surface and Interface Analysis 31(7), 593-598.

Miller, M.K. & Russell, K.F. (2007). Performance of a local electrode atom probe. Surface and Interface Analysis 39(2-3), 262-267.

Miller, M.K., Russell, K.F. & Thompson, G.B. (2005). Strategies for fabricating atom probe specimens with a dual beam FIB. Ultramicroscopy 102(4), 287-298.

Muller, D.J. & Dufrene, Y.F. (2008). Atomic force microscopy as a multifunctional molecular toolbox in nanobiotechnology. Nature Nanotechnology 3(5), 261-269.

Muller, E.W. & Bahadur, K. (1956). FIELD IONIZATION OF GASES AT A METAL SURFACE AND THE RESOLUTION OF THE FIELD ION MICROSCOPE. Physical Review 102(3), 624-631.

Negrila, C.C., Cotirlan, C., Ungureanu, F., Logofatu, C. & Lazarescu, R. (2008). ARXPS analysis of silicon oxide films. J. Optoelectron. Adv. Mater. 10(6), 1379-1383.

Ogletree, D.F., Carpick, R.W. & Salmeron, M. (1996). Calibration of frictional forces in atomic force microscopy. Review of Scientific Instruments 67(9), 3298-3306.

Ruan, J.-A. & Bhushan, B. (1994). Atomic-scale friction measurements using friction-force microscopy. Part I. General principles and new measurement techniques. Journal of Tribology 116(2), 378-388.

Samori, P. (2004). Scanning probe microscopies beyond imaging. Journal of Materials Chemistry 14(9), 1353-1366.

Seidman, D.N. (2007). Three-dimensional atom-probe tomography: Advances and applications. Annual Review of Materials Research 37, 127-158.

Sirghi, L., Kylian, O., Gilliland, D., Ceccone, G. & Rossi, F. (2006). Cleaning and hydrophilization of atomic force microscopy silicon probes. Journal of Physical Chemistry B 110(51), 25975-25981.

Stender, P., Heil, T., Kohl, H. & Schmitz, G. (2009). Quantitative comparison of energy-filtering transmission electron microscopy and atom probe tomography. Ultramicroscopy 109(5), 612-618.

Szlufarska, I., Chandross, M. & Carpick, R.W. (2008). Recent advances in single-asperity nanotribology. J. Phys. D-Appl. Phys. 41(12), 39.

Thompson, G.B., Miller, M.K. & Fraser, H.L. (2004). Some aspects of atom probe specimen preparation and analysis of thin film materials. Ultramicroscopy 100(1-2), 25-34.

Thompson, K., Larson, D.J., Ulfig, R.M., Bunton, J.H. & Kelly, T.F. (2006). Analyzing Si-based structures in 3D with a laser-pulsed local electrode atom probe. Solid State Technol. 49(6), 65-+.

Tomizuka, H. & Ayame, A. (1995). A GRAPHICAL ANALYSIS OF TRANSIENT-RESPONSE CURVES AT AN EARLY-STAGE IN SIMS DEPTH PROFILING USING A (CS+)-C-133 BEAM. Appl. Surf. Sci. 89(3), 281-288.

Torii, A., Sasaki, M., Hane, K. & Okuma, S. (1996). A method for determining the spring constant of cantilevers for atomic force microscopy. Measurement Science & Technology 7(2), 179-184.

Tourek, C. & Sundararajan, S. (2009). Study of Atomic Force Microscopy Probes Using a Local Electrode Atom Probe Microscope. pp. 290-291. Cambridge Journals Online.

Villarrubia, J.S. (1997). Algorithms for scanned probe microscope image simulation, surface reconstruction, and tip estimation. J. Res. Natl. Inst. Stand. Technol. 102(4), 425-454.

Wetzel, A., Socoliuc, A., Meyer, E., Bennewitz, R., Gnecco, E. & Gerber, C. (2005). A versatile instrument for in situ combination of scanning probe

microscopy and time-of-flight mass spectrometry. Review of Scientific Instruments 76(10).

Williams, P.M., Shakesheff, K.M., Davies, M.C., Jackson, D.E., Roberts, C.J. & Tendler, S.J.B. (1996). Blind reconstruction of scanning probe image data. Journal of Vacuum Science and Technology B 14(2), 1557-1562.

CHAPTER 4. ANALYSIS OF THE NEAR-APEX REGIONS OF SCANNING PROBE MICROSCOPY TIPS USING ATOM PROBE TOMOGRAPHY

Modified from a paper submitted to *Ultramicroscopy*

Christopher J. Tourek, Sriram Sundararajan

4.1 Abstract

It is well recognized that the geometry and chemistry of the near-apex region of a scanning probe microscope (SPM) tip greatly affects the tip-sample interactions and consequently the resulting data. In this paper, we report the near-atomic scale characterization of a range of commercially available specialized SPM tips using laser-assisted atom probe tomography (APT). The tips studied include Si tips with hard coatings for wear and nanoindentation studies as well as constant diameter metallic needle tips used for bioanalytical applications and electric force microscopy. The results show that uncoated Si tips along with Si_3N_4 and DLC coated Si tips can be successfully analyzed. Constant diameter Ag_2Ga nanoneedle tips could also be successfully analyzed. The Si_3N_4 coated tips required a higher laser power than Si and tend to field evaporate in various Si_xN_y compounds. The DLC coated tips also required a high tip temperature and laser power to achieve consistent field evaporation and

exhibited mostly C_3^{++}, C^{+} and C^{++}. The coating showed hydrocarbons at higher concentrations at evenly spaced intervals through the coating thickness. The Ag_2Ga tips showed an overall composition close to bulk, however the reconstruction showed a segregated structure of Ga rich and depleted areas. This study demonstrates that APT can help analyze surface and interfacial phenomena that occur at the near-apex regions of SPM tips.

4.2 Introduction

Over the past 25 years, scanning probe microscopy (SPM), and more specifically atomic force microscopy (AFM), has grown into a powerful tool in the fields of nanotechnology and nanoscience for the preparation and analysis of materials, nanostructures and their functionality [1-4]. Since its invention the basic principle of AFM/SPM – measuring a specific interaction between an ultra-sharp tip and a material's surface to obtain structural and/or functional information, has generated a whole range of techniques such as friction force microscopy, nanoindentation, electrical force microscopy and scanning probe lithography, to name a few. Using specialized tips and measuring conditions, a whole range of data can be measured using these techniques [5-10].

It is well recognized that the geometry and chemistry of the near-apex regions of a SPM tip greatly affect the tip-sample interactions and consequently the resulting data. Several techniques to measure the geometry of the tip exist and

have been used widely by researchers, ranging from electron microscopy [11] to using tip characterizer samples and reconstruction algorithms on the resulting images [12-14]. Obtaining chemistry and material structure at the near-apex regions of an SPM tip, however is more challenging. Few techniques exist that are capable of realizing such a small analytical spot size. Researchers have used XPS, TOF-SIMS and contact angle measurements on SPM cantilevers in order to quantify organic contamination levels. These studies then made the assumption that the same contaminants exist on the tip as well [15-17]. SPM has also been combined with time of flight mass spectrometry in vacuum to assess the chemistry of the tip in-situ [18, 19]. More recently, three dimensional atom probe tomography (APT) has been used to directly interrogate the material structure and chemistry of the near-apex regions of Si SPM tips at the near-atomic scale [20].

APT is a technique capable of concurrently determining three dimensional material structure and chemistry at near-atomic resolution which has seen expanding use in science and engineering fields [21-23]. APT works on the phenomenon of field evaporation, by which surface atoms of a needle-shaped specimen are ionized in ultra high vacuum and subsequently desorbed by an electric field. The use of laser-assisted APT has allowed the investigation of non-conductive specimens where a pulsed laser aimed at the specimen is used to realize the field evaporation. Detailed descriptions of the physical principle and

performance of the method can be found in various books and review articles [21, 24].

In this paper, we report the near-atomic scale characterization of a range of commercially available specialized SPM tips using laser-assisted APT. The tips studied include Si tips with hard coatings for wear and nanoindentation studies [1, 25] as well as constant diameter metallic needle tips used for bioanalytical applications, nanolithography, and electric force microscopy studies [26].

4.3 Methods and Materials

The commercially available SPM tips investigated possessed geometry suitable for analysis by APT. The required geometry consists of a sharp needle shape with a tip radius ideally less than 100 nm with smooth sides to create a uniform electric field and a cantilever stiffness greater than 25 N/m to minimize bending of the cantilever in the electric field [20]. In addition to uncoated Si (100) tips, two other types of tips were analyzed - Si tips with hard coatings and a constant diameter metallic nanoneedle tip. Here uncoated NSC15 model (MikroMasch) Si tips having a conical tip shape and nominal normal stiffness of 40 N/m were used. The tips are oriented along the Si (100) direction and n-type doped with phosphorus. Two of the Si tip models with hard coatings, NSC15 LS and NSC15 Si_3N_4 (MikroMasch), are NSC15 tips CVD coated with different thicknesses of Si_3N_4 coatings resulting in nominal radii of 30 and 20 nm

respectively. The third coated tip model, DCP20 (NT-MDT available through K-Tek Nanotechnology), is a boron doped Si tip ion beam deposition coated with diamond-like carbon (DLC) exhibiting a nominal tip radius of 60 nm and normal stiffness of 65N/m. The metallic nanoneedles analyzed were Ag_2Ga NaugaNeedles^{TM} (NaugaNeedles) with a nominal stiffness of 40N/m having a 1um long 50nm constant diameter needle at the apex of an AFM tip.

The tips were analyzed as received using a commercially available atom probe microscope (LEAP 3000X Si, Cameca Instruments Inc.) in pulsed laser mode. AFM tips were loaded into the atom probe microscope using a clip holder (Cameca Instruments Inc.), which facilitated analysis of the AFM tip without the need for permanent mounting. The APT parameters for the analyses are shown in Table 1.

Table1. Parameters for APT analysis of the various SPM tips. All samples were run in pulsed laser mode at 200 kHz and 0.5% evaporation rate.

Tip Type	Material	Sample Temperature (K)	Laser Power (nJ)
NSC15	Si(100)	50	0.3
NSC15 Si3N4	Si3N4 on Si(100)	50	0.9
NSC15 LS	Si3N4 on Si(100)	100	1.2
DCP20	DLC on Si(100)	125	1.3
NaugaNeedle^{TM}	Ag2Ga	50	0.3

4.4 Results and Discussion

4.4.1 Uncoated Si tips

Figure 1 shows a typical mass spectrum of an uncoated NSC15 Si tip obtained from APT analysis. The assumed Si^{+}, Si^{++}, and Si_2^{+} peaks along with O^{+}, O_2^{+}, SiO^{++}, SiO^{+}, SiO_2^{+}, Si_2O^{++}, and Si_2O^{+} indicative of a native oxide are seen in the spectrum. This native oxide layer was found to have a constant concentration zone of 1.5nm with an intermixing zone of 0.5nm [27]. Also seen are Al^{+}, Al^{++}, AlO^{+} and AlO^{++} which likely arise from the deposition of Al on the backside of the cantilever to improve reflectivity in AFM experiments. At the beginning of field evaporation are small amounts of C^{+}, C^{++}, C^{+++}, F^{+} and F++ which is distinctive of CF chain contamination at the tip apex and only seen on the uncoated NSC15 tips.

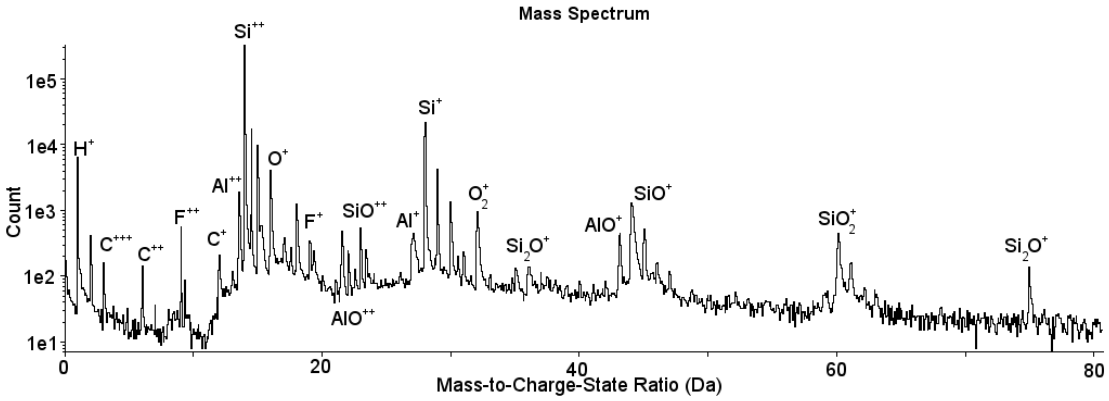

Figure 1. Mass spectrum from APT analysis of an uncoated Si NSC15 AFM tip. Si along with its native oxide are readily seen. There are also indications of CF chain contamination that were seen at the beginning of field evaporation.

4.4.2 Tips with hard coatings

4.4.2.1 Si3N4 coated tips

Silicon nitride (Si_3N_4) coatings are used as hard coatings to minimize wear and tips with this coating are typically used for nanotribological studies. Two different commercially available Si_3N_4 coated NSC15 tips (NSC15 LS and NSC15 Si_3N_4) were analyzed in this study. For these tips, the APT run was started at suitable parameters for Si analysis (0.3 nJ laser pulse 50K) but when the voltage had risen to a point that increased the likelihood of a cantilever fracture (~6000V) and no evaporation of Si_3N_4 was seen the laser power was increased slowly until Si_3N_4 was seen. The threshold laser power observed for consistent field evaporation of Si_3N_4 was 0.9 nJ. Figure 2 shows a typical mass spectrum obtained from the Si_3N_4 coated tips at this setting. There was no discernible difference in chemical composition between the two tips indicating a very similar coating chemistry. The spectrum shows Si peaks along with multiple compounds of Si_xN_y. These Si_xN_y compounds are responsible for the higher laser power necessary to induce field evaporation compared to silicon owing to the stronger bonding energy between S-N than Si-Si (355 vs 222kJ/mol). However, the fact that Si and N have mass to charge ratios that are multiples of each other, 28 and 14 respectively, makes it difficult to determine the specific composition of the higher mass compounds. Also seen is Al from the backside coating similar to that seen in the uncoated NSC15 Si tips. It is noted that the peaks at mass-to-charge

ratios of 18 and 19 are likely from residual outgassing of the APT local electrode and were seen in test runs before and after this data was collected and can be ignored. For the tips, the analysis could not be carried out through the coating interface into the Si bulk, owing to the tip fracturing as the interface was reached. This occurred because the high laser power necessary for Si_3N_4 would likely be too large for Si, resulting in a cascade of atoms field evaporating and stopping the run. To confirm this, the run conditions for Si_3N_4 were tested on a Si tip which showed that the field evaporation was indeed unstable.

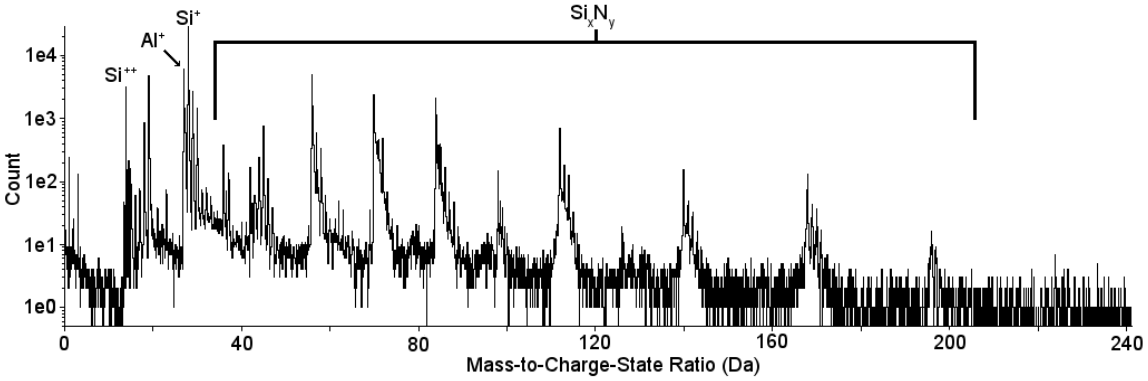

Figure 2. A typical mass spectrum obtained from APT analysis of the Si_3N_4 coated tips. The coating shows presence of several Si_xN_y compounds. Si and N have mass to charge ratios that are multiples of each other (28 and 14) making it difficult to determine composition specifics of the Si_xN_y compounds.

4.4.2.2 DLC coated tips

DLC coatings are also popular for use as wear resistant coatings and DLC coated SPM tips have uses in nanoscale wear and indentation studies. The DLC

coating required a high temperature and laser power to achieve steady field evaporation which agrees well with the high evaporative field of C (103V/nm) and previous studies of DLC materials in by APT [28, 29]. Figure 3 shows a typical mass spectrum of the DLC coating. The evaporation of the coating was dominated by C_3^{++} along with smaller quantities C_2^{+}, C_3^{+}, C_3^{++}, C_4^{+} C_4^{++}, C_5^{+}, C_6^{+}, C_7^{+} throughout. It is noted that there are hydrocarbon groups of $C_2H_3^{+}$, $C_3H_4^{+}$,$C_4H_4^{+}$, $C_4H_6^{+}$, $C_5H_4^{+}$, $C_5H_4^{++}$, and $C_7H_4^{++}$ that are found along with a higher concentration of C^{++} and C^{+} in a few regularly spaced bands in the reconstruction and can be seen in the 1D concentration profile from a 5x5x50nm region down the center of the tip axis in Figure 4. The bands are possibly layers formed during the coating process. Similar to the Si3N4 coated tips the sample fractured at what is assumed to be the interface with Si. This is further confirmed by the thickness of the reconstruction being comparable to the quoted thickness of the coating (approximately 70 nm).

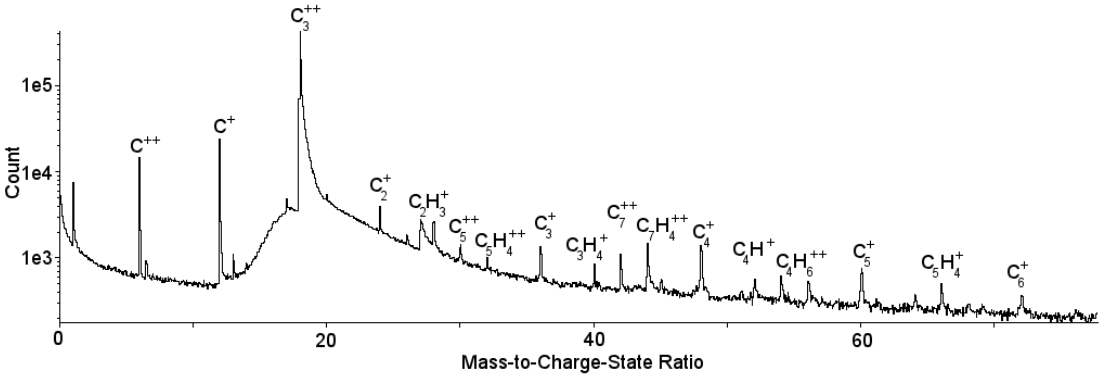

Figure 3. Mass spectrum of a DLC coated AFM tip (DCP20) showing C_3^{++} dominates the field evaporation process and the presence of C_xH_y peaks consistent with amorphous carbon materials.

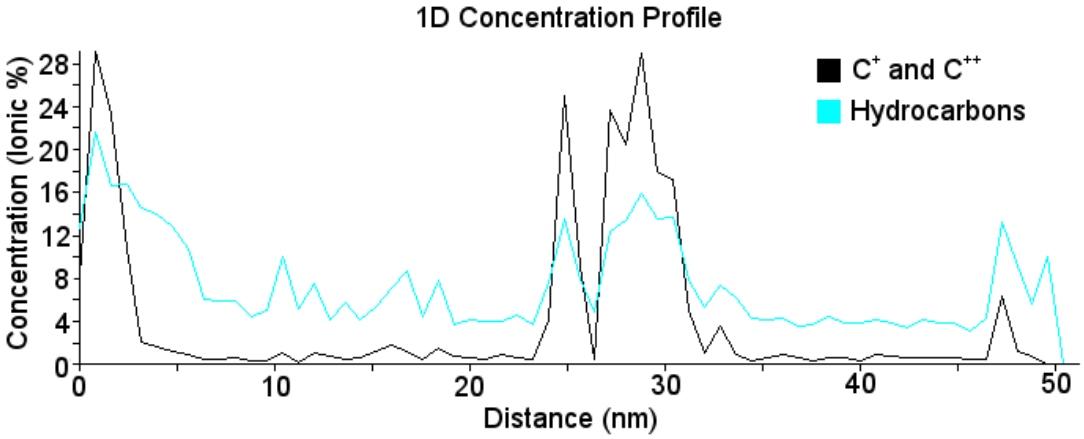

Figure 4. 1D concentration profile showing atomic C and hydrocarbons have a higher concentration at regular intervals through the DLC coating. The profile was taken from a 5x5x50nm region down the center of the tip axis.

4.4.3 Other coated tips

In addition to the coated SPM tips presented above, APT analysis of two other types of coated tips were attempted but did not yield successful field evaporation results. A DLC coated Si tip (Tap300DLC, Budget Sensors) did not exhibit a stable evaporation rate and the tips fractured early in the runs. This is attributed to the non-uniform faceted tip shape exhibited by the tip, as shown in Figure 5, which can lead to a nonuniform electric field. APT runs on NSC15 Si tips coated with Ti-Pt (MikroMasch) typically used for electric force microcopy were also unsuccessful. During field evaporation the coating evaporated in cascades instead of a controlled manor as evidenced by multiple sharp increases in the evaporation rate. This instability can be attributed to large differences in the fields needed to evaporate the outer Pt coating, the underlying Ti coating and Si (45, 26, 33V/nm respectively). The change from a material needing a high field to one needing a much lower field can lead to the underlying material evaporating in an unstable manner due to the high field already present to evaporate the topmost material.

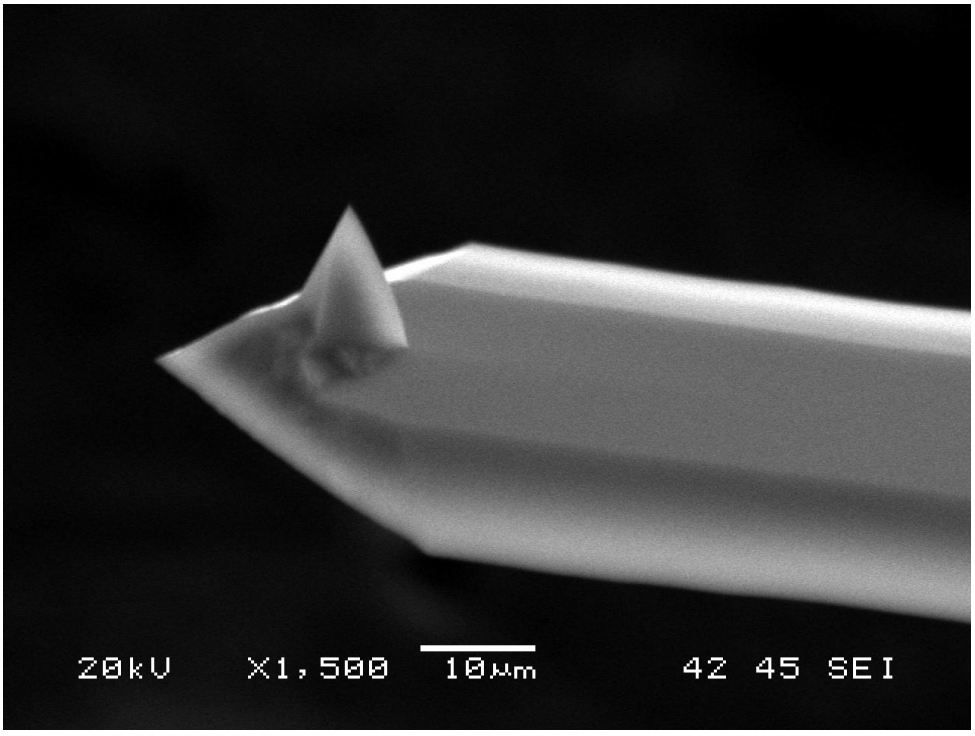

Figure 5. SEM image of a Tap300DLC showing the non-symmetric faceted tip shape, which can exhibit non-uniform electric fields and thus render APT analysis difficult.

4.4.4 Metallic needle tips

An interesting type of AFM tip is the constant diameter metallic needle, which with its conductive properties, is well suited to performing bioanalytical studies, Kelvin force microscopy, electrical force microscopy and scanning probe lithography [26]. Examined here is a NaugaNeedle^{TM}, a novel metallic needle that is formed by inserting a Ag coated AFM probe into a droplet of liquid Ga and drawing it out. This process can create constant diameter needles with a

composition of Ag_2Ga of lengths from 1um to over 30um in length [26]. APT analysis was successful at lower laser power settings than that for the hard coatings, which is consistent with the low fields required for evaporation of Ag and Ga (24 and 15 V/nm respectively). The bulk composition of 70% Ag, 30% Ga from APT shows a slightly higher concentration of Ag compared to the expected values for Ag_2Ga. Upon closer examination of the reconstruction of the data, it can be seen that Ag and Ga are segregated into rich and depleted zones. Figure 6 (a) shows a top view of the reconstruction along with isoconcentration surfaces of the Ga rich zones (b) and an example 1-D concentration profile through one of the Ga rich zones (c). The percentage of Ga in the rich zones ranges from 60 to 90%.

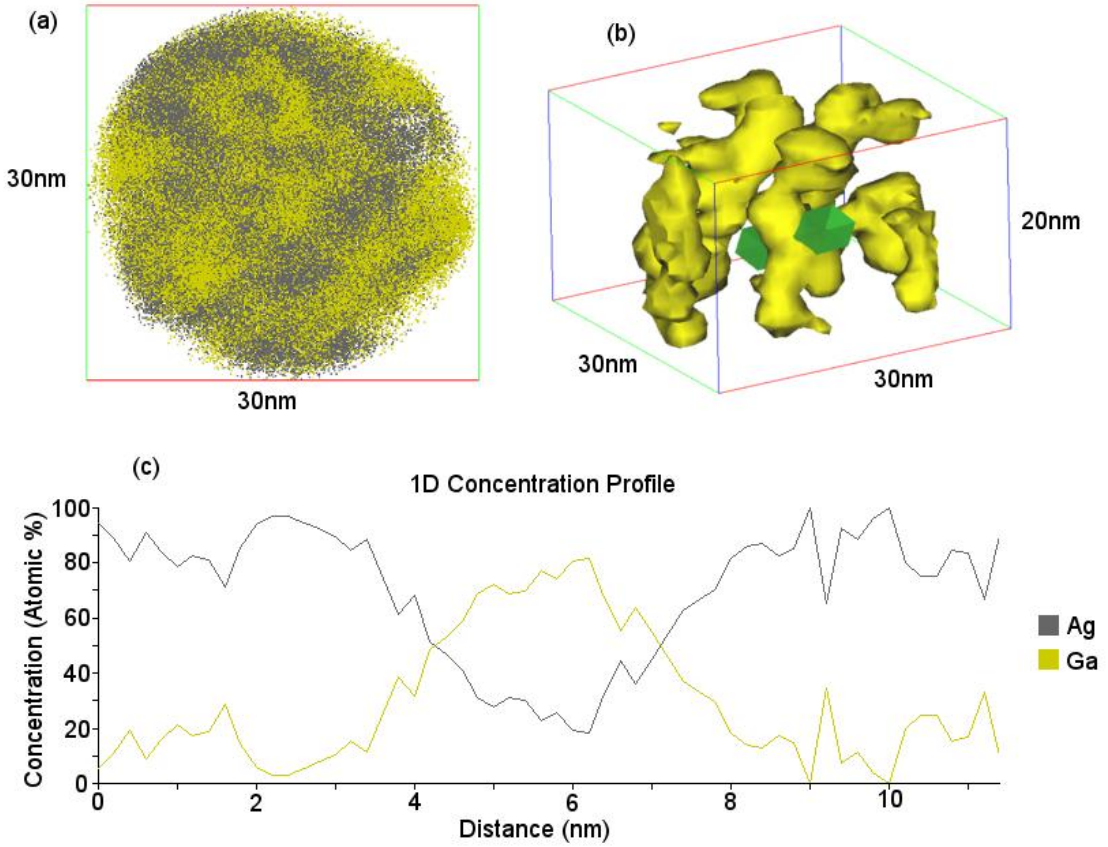

Figure 6. Top view of a NaugaNeedle^{TM} APT reconstruction (a) along with isoconcetration surfaces highlighting the Ga rich zones (b), and a 1D concentration profile (c) along the long axis of the region shown in (b).

4.5 Conclusions

In this study, the near-apex regions of several commercially available SPM tips were successfully analyzed at the near-atomic scale using atom probe tomography. Conical Si tips, both uncoated and coated with Si_3N_4 and DLC coatings exhibited stable field evaporation and chemical mapping. The Si_3N_4

coated tips required a higher laser power than uncoated Si and tended to field evaporate in various Si_xN_y compounds. The DLC coated tips required a high tip temperature and laser power to achieve consistent field evaporation and exhibited mostly C_3^{++}, C^+ and C^{++} species. The coating also showed the presence of hydrocarbons at higher concentrations at evenly spaced intervals through the coating thickness. Constant diameter Ag_2Ga needle tips were also readily analyzed and showed an overall composition close to bulk Ag_2Ga. However the reconstruction showed segregated structure of Ga rich and depleted areas.

It is noted that in almost all the runs on the coated tips, stable field evaporation tended to stop as the interface was reached. Caused by the high fields needed to field evaporate the coating materials compared to the Si substrate, this rendered the imaging and analysis of the interface difficult. However the atom-scale analysis method does provide the capability to analyze the surface regions reliably enough to potentially allow detection of surface or near-surface chemical changes. Consequently APT provides researchers with a very powerful tool to analyze surface and interfacial phenomena that occur at the near-apex regions of SPM tips. Examples of studies that can leverage this capability include quantifying contamination in SPM tips and analysis of material transfer or transformation in SPM experiments.

Acknowledgements

Partial funding for this study was provided by grants from the National Science Foundation (Grant no. CBET 0932573) and the W.M. Keck Foundation. The authors would also like to thank Jamie Arnold at MikroMasch for help in selecting and acquiring details on the AFM probes

References

[1] B. Bhushan, J.N. Israelachvili, U. Landman, NANOTRIBOLOGY - FRICTION, WEAR AND LUBRICATION AT THE ATOMIC-SCALE, Nature, 374 (1995) 607-616.

[2] R.W. Carpick, M. Salmeron, Scratching the surface: Fundamental investigations of tribology with atomic force microscopy, Chemical Reviews, 97 (1997) 1163-1194.

[3] P.T. Lillehei, L.A. Bottomley, Scanning probe microscopy, Analytical Chemistry, 72 (2000) 189R-196R.

[4] J. Loos, The art of SPM: Scanning probe microscopy in materials science, Advanced Materials, 17 (2005) 1821-1833.

[5] H.J. Butt, B. Cappella, M. Kappl, Force measurements with the atomic force microscope: Technique, interpretation and applications, Surface Science Reports, 59 (2005) 1-152.

[6] L.C. Giancarlo, G.W. Flynn, Scanning tunneling and atomic force microscopy probes of self-assembled, physisorbed monolayers: Peeking at the peaks, Annual Review of Physical Chemistry, 49 (1998) 297-+.

[7] D.J. Muller, Y.F. Dufrene, Atomic force microscopy as a multifunctional molecular toolbox in nanobiotechnology, Nature Nanotechnology, 3 (2008) 261-269.

[8] P. Samori, Scanning probe microscopies beyond imaging, Journal of Materials Chemistry, 14 (2004) 1353-1366.

[9] Bhushan, Handbook of Micro/Nanotribology Second Edition, 1998.

[10] I. Szlufarska, M. Chandross, R.W. Carpick, Recent advances in single-asperity nanotribology, J. Phys. D-Appl. Phys., 41 (2008) 39.

[11] L.S. Dongmo, J.S. Villarrubia, S.N. Jones, T.B. Renegar, M. Postek, J.F. Song, Experimental test of blind tip reconstruction for scanning probe microscopy, Ultramicroscopy, 85 (2000) 141-153.

[12] V. Bykov, A. Gologanov, V. Shevyakov, Test structure for SPM tip shape deconvolution, Appl. Phys. A-Mater. Sci. Process., 66 (1998) 499-502.

[13] J.S. Villarrubia, Algorithms for scanned probe microscope image simulation, surface reconstruction, and tip estimation, J. Res. Natl. Inst. Stand. Technol., 102 (1997) 425-454.

[14] P.M. Williams, K.M. Shakesheff, M.C. Davies, D.E. Jackson, C.J. Roberts, S.J.B. Tendler, Blind reconstruction of scanning probe image data, Journal of Vacuum Science and Technology B, 14 (1996) 1557-1562.

[15] E. Bonaccurso, G. Gillies, Revealing contamination on AFM cantilevers by microdrops and microbubbles, Langmuir, 20 (2004) 11824-11827.

[16] Y.S. Lo, N.D. Huefner, W.S. Chan, P. Dryden, B. Hagenhoff, T.P. Beebe, Organic and inorganic contamination on commercial AFM cantilevers, Langmuir, 15 (1999) 6522-6526.

[17] L. Sirghi, O. Kylian, D. Gilliland, G. Ceccone, F. Rossi, Cleaning and hydrophilization of atomic force microscopy silicon probes, Journal of Physical Chemistry B, 110 (2006) 25975-25981.

[18] D. Lee, A. Wetzel, R. Bennewitz, E. Meyer, M. Despont, P. Vettiger, C. Gerber, Switchable cantilever for a time-of-flight scanning force microscope, Applied Physics Letters, 84 (2004) 1558-1560.

[19] A. Wetzel, A. Socoliuc, E. Meyer, R. Bennewitz, E. Gnecco, C. Gerber, A versatile instrument for in situ combination of scanning probe microscopy and time-of-flight mass spectrometry, Review of Scientific Instruments, 76 (2005).

[20] C. Tourek, S. Sundararajan, Study of Atomic Force Microscopy Probes Using a Local Electrode Atom Probe Microscope, in, Cambridge Journals Online, 2009, pp. 290-291.

[21] T.F. Kelly, M.K. Miller, Invited review article: Atom probe tomography, Review of Scientific Instruments, 78 (2007) 20.

[22] D.N. Seidman, Three-dimensional atom-probe tomography: Advances and applications, Annual Review of Materials Research, 37 (2007) 127-158.

[23] K. Thompson, D.J. Larson, R.M. Ulfig, J.H. Bunton, T.F. Kelly, Analyzing Si-based structures in 3D with a laser-pulsed local electrode atom probe, Solid State Technol., 49 (2006) 65-+.

[24] M.K. Miller, Atom Probe Tomography Analysis at the Atomic Level, Kluwer Academic/Plenum Publishers, New York, 2000.

[25] M. Petzold, J. Landgraf, M. Futing, J.M. Olaf, APPLICATION OF ATOMIC-FORCE MICROSCOPY FOR MICROINDENTATION TESTING, Thin Solid Films, 264 (1995) 153-158.

[26] M.M. Yazdanpanah, S.A. Harfenist, A. Safir, R.W. Cohn, Selective self-assembly at room temperature of individual freestanding Ag2Ga alloy nanoneedles, Journal of Applied Physics, 98 (2005).

[27] N.N. Greenwood, A. Earnshaw, Chemistry of the Elements, in, Elsevier, 1997, pp. 1344p.

[28] O. Nishikawa, T. Sekine, Y. Ohtani, K. Maeda, Y. Numada, M. Watanabe, Atomic investigation of individual apexes of diamond emitters by a scanning atom probe, J. Vac. Sci. Technol. B, 16 (1998) 836-840.

[29] T.W. Scharf, M.C. Romanes, K.C. Mahdak, J.Y. Hwang, R. Banerjee, R.D. Evans, G.L. Doll, Atomic-scale structure and composition of tungsten carbide reinforced diamondlike carbon films, Appl. Phys. Lett., 93 (2008).

CHAPTER 5. AN ALTERNATIVE METHOD TO DETERMINING OPTICAL LEVER SENSITIVITY IN ATOMIC FORCE MICROSCOPY WITHOUT TIP-SAMPLE CONTACT

Modified from a paper published in *Review of Scientific Instruments*

Christopher J. Tourek, Sriram Sundararajan

5.1 Abstract

Force studies using atomic force microscopy generally require knowledge of the cantilever spring constants and the optical lever sensitivity. The traditional method of evaluating the optical lever sensitivity by pressing the tip against a hard surface can damage the tip, especially sharp ones. Here a method is shown to calculate the sensitivity without having to bring the tip into contact. Instead a sharpened tungsten wire is used to cause a point contact directly onto the cantilever and cause cantilever bending. Using beam theory, the sensitivity thus found can be converted to the equivalent sensitivity that would be obtained using the tip location. A comparison is presented between sensitivity values obtained from the conventional tip contact method and those derived from the wire-based technique for a range of cantilevers in air. It was found that the difference between the calculated sensitivity from the wire-based technique and the sensitivity obtained conventionally was less than 12%. These measurements

indicate the presented method offers a simple alternative approach to obtain optical lever sensitivity without compromising the tip shape.

5.2 Introduction

Since its invention in the early 1980s the atomic force microscope (AFM) has become one of the most powerful tools in the fields of nanoscience and nanotechnology for the preparation and analysis of materials, nanostructures and their functionality.[1-11] An important aspect in many AFM experiments is determining the optical lever sensitivity (sensitivity) which allows the bending of the cantilever to be translated into the vertical deflection (distance) units. Combining the sensitivity and the calibrated normal spring constant[12-15] of the AFM cantilever allows the forces applied to the sample to be calculated. Traditionally the sensitivity is determined by pressing the tip at the end of the cantilever onto a hard surface that is assumed to not deform under the applied load, and observing the slope of the force curve.[16] However, pressing the tip onto a hard surface can result in damage to the tip, especially for sharper tips and tips with functionalizations such as organic films and carbon nanotubes.[17] FIG. 1 shows the change in tip shape that occurred to a sharp silicon tip (series HAR5 from NanoScience Instruments Inc.) while finding the sensitivity in the conventional manner. This change corresponded to a 70% change in the tip radius. Data from other tips with similar initial tip radii also showed shape

change from the traditional sensitivity calibration. NSC15(Mikromasch) showed a tip radius change on the order of 50% and NP-S, silicon nitride tips, (Veeco Instruments) showed a tip radius change of 25%. Researchers have developed noncontact methods to determine the sensitivity. These techniques require measuring the thermal noise spectrum of the cantilever,[18, 19] creating calibration curves for each length of cantilever,[20] changing parts of the optical system,[21] or the use of colloidal tips only.[22] We present here a technique that allows the sensitivity to be evaluated for any AFM tip/cantilever for which the beam bending equations can be determined, without the need for tip-surface contact or modification to a commercial microscope. In this method a sharpened tungsten wire is brought into contact directly onto the cantilever at a point away from the tip, and the sensitivity can be found from the force curve obtained with a correction made for the offset between the contact point and location of the tip. In this article, we present our investigations for commercially available rectangular cantilevers with a range of spring constants.

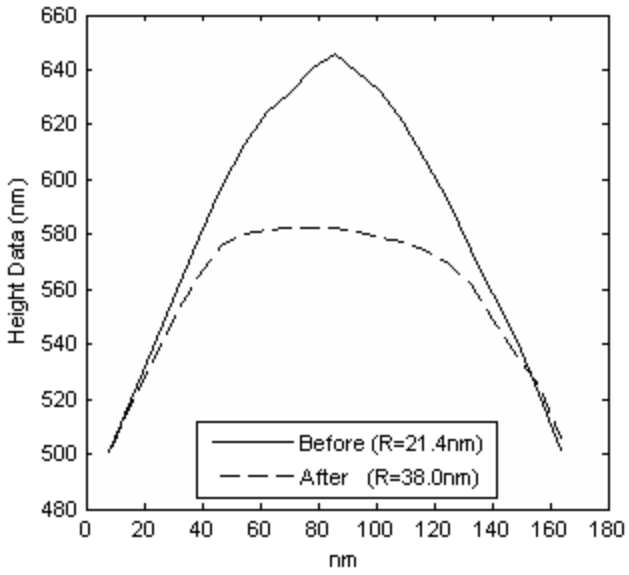

FIG. 1. Comparison of silicon tip shape before and after finding the sensitivity of a HAR5 series cantilever (NanoScience instruments Inc., calibrated normal spring constant of 46 N/m) using the traditional method on a sapphire sample. The tip shape was found by reverse imaging the tip before and after capturing a force curve on sapphire.

5.3 Experimental Methods

The required bending of the cantilever is achieved via a point contact directly on the cantilever rather than by tip-surface contact. The point contact is achieved by a sharpened tungsten wire that is held vertically allowing the cantilever to be brought down into contact for the sensitivity measurement as shown in Fig. 2. The tungsten wire was created using conventional electropolishing, which is used

widely to prepare samples in field emission and atom probe microscopy.[23] To create the tungsten tip used here, a 1cm long 0.305mm diameter tungsten wire was electropolished using 5% NaOH at 4V to obtain a needle shape using a loop electrode [24].

For a rectangular cantilever, beam theory can be used to calculate the change in observed sensitivity caused by moving the contact point along the cantilever and away from the location of the AFM tip. For all discussions here distances will be taken as measured along the cantilever axis from the base of the cantilever towards the end of the cantilever. There are two different alignments of the contact point that must be taken into consideration. First, the situation where the contact point is past the laser reflection point (Fig. 2a), and second, the situation where the contact point is before the laser reflection point (Fig. 2b).

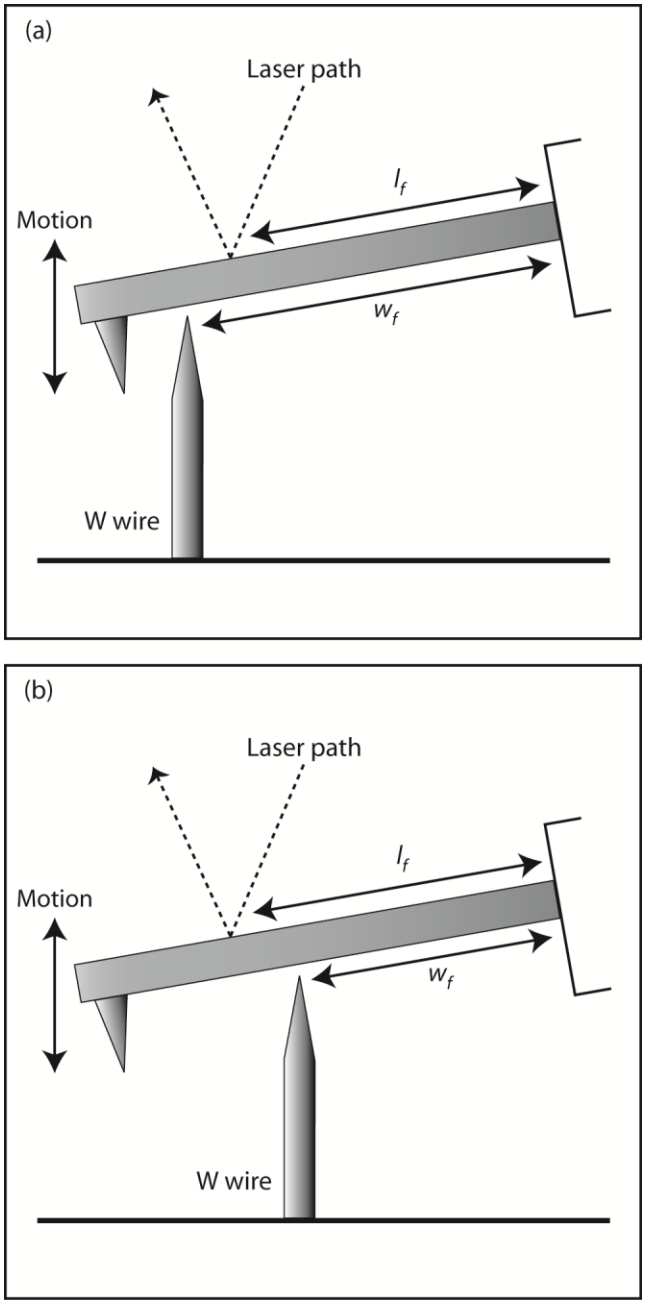

FIG. 2. Schematic of a tungsten wire as the contact point being (a) past the laser reflection and (b) before the reflection. The relevant measured length fractions for the laser position (l_f) and tungsten wire contact (w_f) are also shown.

The parameter of concern is the angle of the cantilever at the laser reflection spot on the cantilever because when a force is applied to the cantilever, the cantilever bends and the reflected light moves through an angle twice the change in the slope of the cantilever at the reflection[16]. For a rectangular cantilever, the equation for the angle of the cantilever at the laser spot θ_p, for the case where the point of contact is past the laser spot (Fig. 2a) is,

$$\theta_p = \frac{P}{2EI}\left(2xl - l^2\right) \qquad (1)$$

where P is the force applied to cantilever at the contact point, E is the elastic constant of the beam, and I is the second moment of area of the beam. Distances l and x identify the locations of the laser spot and contact point respectively, measured from the base of the cantilever. For the case where the wire contact point is before the laser spot (Fig. 2b), the equivalent equation is given by,

$$\theta_b = \frac{Px^2}{2EI} \qquad (2)$$

assuming that the cantilever retains the same angle past the point of contact. The displacement from force applied at the contact point is given by

$$y = \frac{Px^3}{3EI} \qquad (3)$$

By rearranging and substituting Eq. (3) into Eq. (1) and Eq. (2) yields

$$\theta_p = \frac{3y}{\left(2x^3\right)\left(2xl - l^2\right)} \tag{4}$$

$$\theta_b = \frac{3y}{\left(2x\right)} \tag{5}$$

We are generally interested in the sensitivity obtained when the force is applied at the location of the AFM tip. Since the force application point (contact point of tungsten wire) is offset from the AFM tip, we need to account for the corresponding change in cantilever bending (angle) due to this offset. If θ_a and θ_w represent the cantilever angle at the laser spot caused by force application at the AFM tip and the tungsten wire respectively, the percent difference in the cantilever angle at the laser spot caused by this offset is given by

$$\frac{\theta_w - \theta_a}{\theta_a} = \frac{a^3\left(2wl - l^2\right)}{w^3\left(2al - l^2\right)} - 1 \tag{6}$$

$$\frac{\theta_w - \theta_a}{\theta_a} = \frac{a^3}{w\left(2al - l^2\right)} - 1 \tag{7}$$

where *a* is the position of the AFM tip and *w* is the contact position of the tungsten wire. Eq. (6) is for the situation where the tungsten wire contact is past the laser spot (Fig. 2a) and Eq. (7) is for where the tungsten wire contact is before the laser spot (Fig. 2b). Both Eqs. (6) and (7) assume that the AFM tip is at or past the laser spot, which is fairly representative of experimental conditions.

It can be shown that the sensitivity for force application at the AFM tip (S_a) and at the tungsten wire contact (S_w) are related by

$$S_a = S_w\left(1+\frac{\theta_w-\theta_a}{\theta_a}\right) \tag{8}$$

Using Eqs. (6) and (7) in Eq. (8) gives the following equations for the two contact situations in Fig. 2a and 2b respectively:

$$S_a = \left(\frac{a^3\left(2wl-l^2\right)}{w^3\left(2al-l^2\right)}\right)S_w \tag{9}$$

$$S_a = \left(\frac{a^3}{w\left(2al-l^2\right)}\right)S_w \tag{10}$$

It can be shown that if *a, w,* and *l* are substituted for their respective length fractions from the base of the cantilever a_f, w_f, and l_f respectively, Eq. (9) and Eq. (10) become:

$$S_a = \left(\frac{{a_f}^3\left(2w_f l_f-{l_f}^2\right)}{{w_f}^3\left(2a_f l_f-{l_f}^2\right)}\right)S_w \tag{11}$$

$$S_a = \left(\frac{{a_f}^3}{w_f\left(2a_f l_f-{l_f}^2\right)}\right)S_w \tag{12}$$

The use of length fractions allows images captured from the optics of the AFM to be used to determine the necessary parameters for the calculations (a_f,

w_f, and l_f) without the need for calibrating the distances in the images. Thus using Eqs. (11) and (12) we can calculate the sensitivity caused by contact occurring at the AFM tip location (S_a) from the sensitivity obtained experimentally from contact with a tungsten wire directly onto the cantilever (S_w).

In order to verify the application of Eqs. (11) and (12), experiments were carried out on tipless rectangular cantilevers with a range of lengths and normal spring constants using a Dimension 3100 AFM with a Nanoscope IV controller (Veeco Instruments, Santa Barbara). The spring constants used in this study were 0.15 N/nm, 2.9 N/nm and 59 N/nm as measured by the Sader method.[15] Experiments were also carried out on 3 silicon-probe cantilevers (HAR5 from Nanoscience Instruments Inc) with calibrated spring constants of 35-41 N/m. Each cantilever was loaded into the AFM as normal and a frequency sweep was done to verify the resonance characteristics and check for potential problems with the cantilever. Force curves where then obtained by aligning the cantilever over the tungsten wire using the optics of the AFM and engaging on the tungsten wire. High resolution images were also captured of the alignments and used to determine the positions along the cantilever of the laser spot, AFM tip, and the tungsten wire contact for the calculations.

5.4 Results and Discussion

To analyze the validity of Eqs. (11) and (12) to predict the sensitivity (S_a) from the measured sensitivity (S_w) experiments with a tungsten wire were first performed on tipless cantilevers. The contact point with the tungsten wire was varied along the length of each cantilever to realize 4 differing length fractions (w_f) as listed in Table 1. Table 1 also lists the various quantities for the cantilevers used and the obtained sensitivities S_w (measured) and S_a (calculated). In lieu of the sensitivity that would be obtained conventionally using an AFM tip, the sensitivity (S_w') obtained from the farthest contact point from the base of the cantilever (w_f') was used as the reference sensitivity to compare the other calculated sensitivity (S_a) values against. Also listed is the error associated with the sensitivity values estimated using error propagation. This includes uncertainties associated with estimating distances for the laser spot (±3%) and tungsten wire (±2%) contact locations from the digital photos of the cantilevers as well as random error associated with estimating the sensitivity from the force curves (using the mean and standard deviation from a sample of 5 sensitivity estimates for each contact location). From Table 1, it can be seen that the difference between the calculated sensitivities (S_a) for various values of w_f and S_w and the reference sensitivity (S_w') is less than 6% for all the cantilevers tested. Fig. 3b shows this difference visually.

Table 1. Results from tipless cantilever sensitivity experiments. Obtained values are shown along with associated error. The error was calculated using error propagation and includes error inherent in finding the distances from images and finding the sensitivity from the force curves.

Tipless Cantilever	Normal spring constant[a], k (N/m)	Length fraction of laser spot, l_f	Farthest length fraction for contact point, w_f'	Length fraction of tungsten wire position, w_f	Measured sensitivity, S_w (nm/V)	Reference sensitivity corresponding to w_f', S_w' (nm/V)	Calculated sensitivity[b], S_a (nm/V)	% Difference between S_a and S_w'
1	0.15	0.91	0.87	0.83	214.16	230.60	225.58 ± 4.28	2.18 % ± 2.00
				0.74	198.48		235.91 ± 4.52	-2.30 % ± 2.11
				0.64	176.80		242.18 ± 4.97	-5.02 % ± 2.30
2	2.9	0.81	0.90	0.82	79.37	84.45	88.93 ± 2.65	-5.31 % ± 3.31
				0.71	67.93		87.67 ± 3.04	-3.82 % ± 3.75
				0.66	60.59		84.36 ± 2.65	0.11 % ± 3.30
3	59	0.68	0.82	0.72	41.34	47.70	48.19 ± 2.18	-1.04 % ± 4.68
				0.59	34.63		49.15 ± 2.54	-3.04 % ± 5.42
				0.55	33.16		50.49 ± 2.72	-5.85 % ± 5.79

[a]found using Sader's method [15]

[b]Calculated using Eqs. (11) or (12) depending on if l_f was larger or smaller than w_f

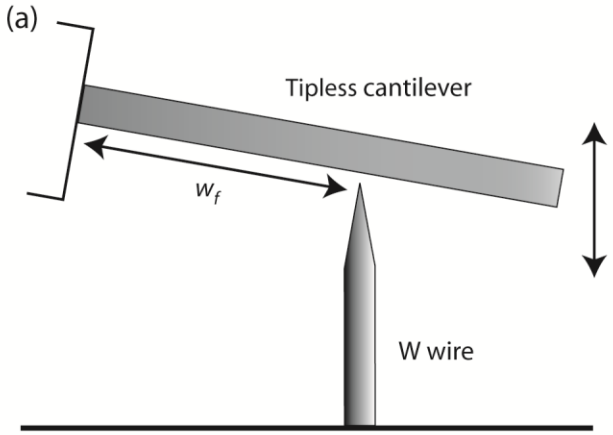
(a)
Tipless cantilever
w_f
W wire

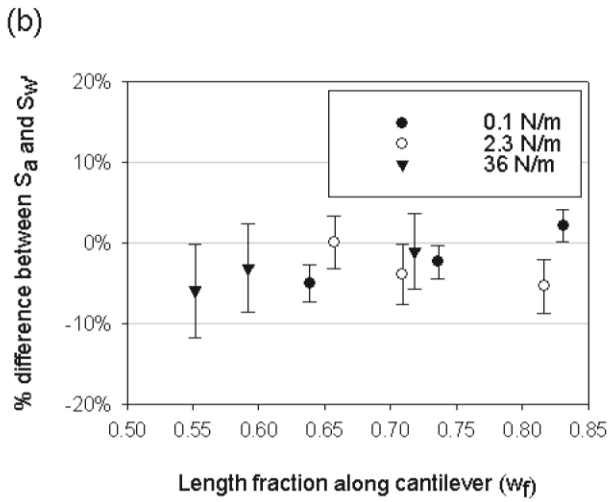
(b)
% difference between S_a and $S_{a'}$
20%
10%
0%
-10%
-20%
0.50
0.55
0.60
0.65
0.70
0.75
0.80
0.85
0.1 N/m
2.3 N/m
36 N/m
Length fraction along cantilever (w_f)

FIG. 3. (a) A schematic of the line up showing the length fraction for the tungsten wire contact position (w_f) and (b) a graph showing the percent difference between calculated sensitivity (S_a) and the reference sensitivity (S_w') for the tipless cantilevers as a function of w_f.

Next, experiments were performed on Si probe cantilevers (HAR5) to compare the sensitivity values obtained from the tungsten wire contact method (S_a) with the traditional tip contact method against a sapphire sample (S_a'). For each HAR5 cantilever, three contact positions (w_f) were used to obtain measured sensitivity (S_w) and calculate the true sensitivity (S_a). The results for 3 different cantilevers are shown in Table 2. Results from HAR5 cantilever sensitivity experiments. Obtained values are shown along with associated error. The error was calculated using error propagation and includes error inherent in finding the distances from images and finding the sensitivity from the force curves.

HAR5 Cantilever	Normal spring constant[a], k (N/m)	Length fraction of laser spot, l_f	Farthest length fraction for contact point, w_f'	Length fraction of tungsten wire position, w_f	Measured sensitivity, S_w (nm/V)	Reference sensitivity corresponding to w_f' S_a' (nm/V)	Calculated sensitivity[b], S_a (nm/V)	% Difference between S_a and S_a'
1	35	0.82	0.93	0.83	61.51	75.25	74.41 ± 1.88	1.12 % ± 2.77
				0.78	57.72		74.05 ± 1.93	1.58 % ± 2.82
				0.57	46.06		80.28 ± 2.19	-6.69 % ± 3.19

2	39	0.77	0.94	0.75	52.34	77.28	67.95 ± 1.92	11.59 % ± 2.61
				0.64	46.14		70.15 ± 1.89	8.08 % ± 2.59
				0.53	38.74		70.89 ± 2.07	6.95 % ± 2.81
3	41	0.83	0.94	0.81	59.91	70.95	70.16 ± 1.65	1.11 % ± 2.72
				0.74	54.88		70.45 ± 1.72	0.70 % ± 2.80
				0.64	47.28		70.77 ± 1.96	0.26 % ± 3.10

[a]found using Sader's method [15]

[b]Calculated using Eqs. (11) or (12) depending on if l_f was larger or smaller than w_f

. It was found that if the point of contact is kept past the mid-point of the cantilever length (w_f > 0.5), the percent difference from the calculated sensitivity to the reference sensitivity (S_a') is less than 12%. The data indicate that the method described here is effective in determining the sensitivity for AFM cantilevers. We note that although rectangular cantilevers were used to demonstrate the method, the technique will work for any cantilever geometry for which the bending behavior in response to a point load can be determined.

Table 2. Results from HAR5 cantilever sensitivity experiments. Obtained values are shown along with associated error. The error was calculated using error propagation and includes error inherent in finding the distances from images and finding the sensitivity from the force curves.

HAR5 Cantilever	Normal spring constant[a], k (N/m)	Length fraction of laser spot, l_f	Farthest length fraction for contact point, w_f'	Length fraction of tungsten wire position, w_f	Measured sensitivity, S_w (nm/V)	Reference sensitivity corresponding to w_f' S_a' (nm/V)	Calculated sensitivity[b], S_a (nm/V)	% Difference between S_a and S_a'
1	35	0.82	0.93	0.83	61.51	75.25	74.41 ± 1.88	1.12 % ± 2.77
				0.78	57.72		74.05 ± 1.93	1.58 % ± 2.82
				0.57	46.06		80.28 ± 2.19	-6.69 % ± 3.19
2	39	0.77	0.94	0.75	52.34	77.28	67.95 ± 1.92	11.59 % ± 2.61
				0.64	46.14		70.15 ± 1.89	8.08 % ± 2.59
				0.53	38.74		70.89 ± 2.07	6.95 % ± 2.81
3	41	0.83	0.94	0.81	59.91	70.95	70.16 ± 1.65	1.11 % ± 2.72
				0.74	54.88		70.45 ± 1.72	0.70 % ± 2.80
				0.64	47.28		70.77 ± 1.96	0.26 % ± 3.10

[a]found using Sader's method [15]

[b]Calculated using Eqs. (11) or (12) depending on if l_f was larger or smaller than w_f

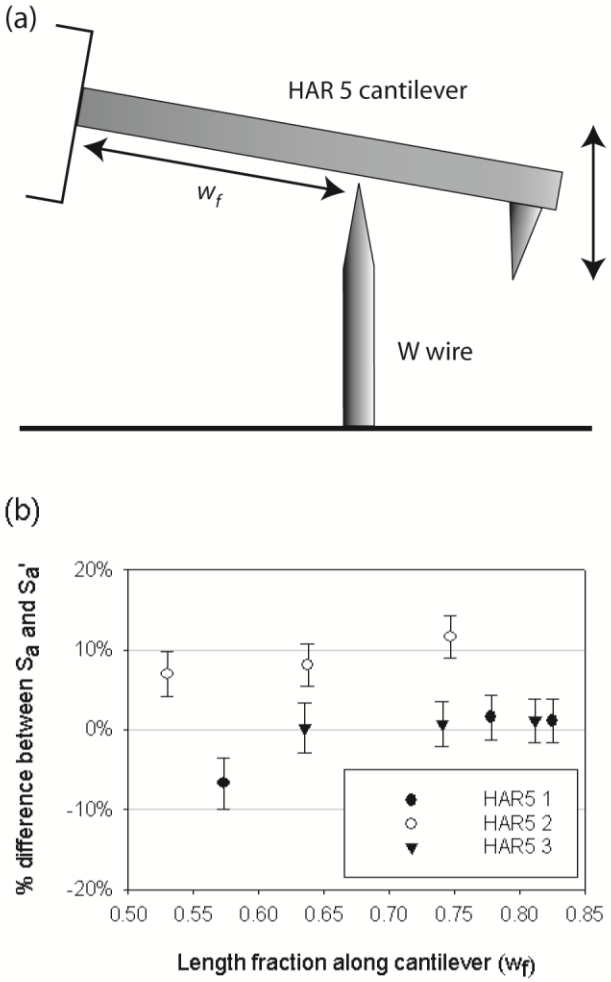

FIG. 4. (a) A schematic of the line up showing the length fraction for the tungsten wire contact position (w_f) and (b) a graph showing the percent difference between the calculated sensitivity (S_a) and the reference sensitivity (S_a') for the HAR5 cantilevers as a function of w_f.

It should also be noted that one generally assumes during optical level sensitivity determinations that the contacting surface undergoes negligible deformation. In our experiments, the load needed to buckle the wire was on the order of Newtons, while the loads applied in the experiments were on the order of μN. The end of the tungsten wire had a typical radius of 5um which allowed a sufficient contact area to not damage the cantilever or the wire. Furthermore, this radius allowed for the wire end to be seen in the optics of the AFM while remaining small enough to maneuver without touching the AFM tip. It is also noted that the same tungsten wire was used for all experiments and checked between experiments for damage using an optical microscope.

5.5 Conclusions

The traditional way of finding the sensitivity of an AFM cantilever by pressing its tip against a hard surface and finding the slope of the force curve can damage sharp tips. A method was shown to calculate the optical lever sensitivity of AFM cantilevers without having to initiate tip-surface contact. Instead a reusable sharpened tungsten wire was used to generate a point contact directly onto the cantilever and cause bending. It was found that the difference between the calculated sensitivity using this method and the sensitivity determined conventionally was less than 12% for rectangular cantilevers. The presented

method offers a simple alternative approach to obtain optical lever sensitivity which is especially useful for studies where tip shape cannot be compromised.

Acknowledgements:

Funding for this study was provided by a grant from the National Science Foundation (Grant no. 0932573). The authors would also like to thank Curtis Mosher, Associate Scientist at the Roy J. Carver Laboratory for Ultrahigh Resolution Biological Microscopy at Iowa State University, for many helpful discussions.

References

1. R. Berger, H. J. Butt, M. B. Retschke and S. A. L. Weber, Macromolecular Rapid Communications 30 (14), 1167-1178 (2009).

2. A. A. Gewirth and B. K. Niece, Chemical Reviews 97 (4), 1129-1162 (1997).

3. M. E. Greene, C. R. Kinser, D. E. Kramer, L. S. C. Pingree and M. C. Hersam, Microscopy Research and Technique 64 (5-6), 415-434 (2004).

4. H. G. Hansma and L. Pietrasanta, Current Opinion in Chemical Biology 2 (5), 579-584 (1998).

5. U. Hartmann, Annual Review of Materials Science 29, 53-87 (1999).

6. J. K. H. Horber and M. J. Miles, Science 302 (5647), 1002-1005 (2003).

7. P. T. Lillehei and L. A. Bottomley, Analytical Chemistry 72 (12), 189R-196R (2000).

8. J. Loos, Advanced Materials 17 (15), 1821-1833 (2005).

9. E. Oesterschulze, in Advances in Imaging and Electron Physics, Vol 118 (2001), Vol. 118, pp. 129-206.

10. M. A. Poggi, E. D. Gadsby, L. A. Bottomley, W. P. King, E. Oroudjev and H. Hansma, Analytical Chemistry 76 (12), 3429-3443 (2004).

11. P. Samori, Journal of Materials Chemistry 14 (9), 1353-1366 (2004).

12. D. S. Golovko, T. Haschke, W. Wiechert and E. Bonaccurso, Rev. Sci. Instrum. 78 (4), 6 (2007).

13. B. Y. Liu, Y. Yu, D. K. Yao and J. Y. Shao, Rev. Sci. Instrum. 80 (6), 9 (2009).

14. S. M. Notley, S. Biggs and V. S. J. Craig, Rev. Sci. Instrum. 74 (9), 4026-4032 (2003).

15. J. E. Sader, J. W. M. Chon and P. Mulvaney, Rev. Sci. Instrum. 70 (10), 3967-3969 (1999).

16. H. J. Butt, B. Cappella and M. Kappl, Surf. Sci. Rep. 59 (1-6), 1-152 (2005).

17. C. L. Cheung, J. H. Hafner and C. M. Lieber, Proceedings of the National Academy of Sciences of the United States of America 97 (8), 3809-3813 (2000).

18. P. Attard, T. Pettersson and M. W. Rutland, Rev. Sci. Instrum. 77 (11), 4 (2006).

19. M. J. Higgins, R. Proksch, J. E. Sader, M. Polcik, S. Mc Endoo, J. P. Cleveland and S. P. Jarvis, Rev. Sci. Instrum. 77 (1), 5 (2006).

20. N. P. Dcosta and J. H. Hoh, Rev. Sci. Instrum. 66 (10), 5096-5097 (1995).

21. L. K. Brar, M. Paranjape, A. Guha and A. K. Raychaudhuri, Curr. Sci. 83 (10), 1197-1199 (2002).

22. V. S. J. Craig and C. Neto, Langmuir 17 (19), 6018-6022 (2001).

23. M. K. Miller, Atom Probe Tomography Analysis at the Atomic Level. (Kluwer Academic/Plenum Publishers, New York, 2000).

24. A. J. Melmed, J. Vac. Sci. Technol. B 9 (2), 601-608 (1991).

CHAPTER 6. CHARACTERIZATION OF MATERIAL TRANSFER ONTO AN ATOMIC FORCE MICROSCOPE TIP RESULTING FROM NANOSCALE DRY SLIDING USING ATOM PROBE TOMOGRAPHY

Modified from a paper for *Wear of Materials*

Christopher J. Tourek, Sriram Sundararajan

6.1 Abstract

Atomic force microscopy (AFM) is used extensively to investigate nanotribological and nanomechanical phenomena. The ability to characterize the structure and chemistry of transferred or newly generated material at the near-apex regions of AFM tips can provide new insights into a range of nanoscale interfacial phenomena including friction, adhesion, wear and corrosion. Atom probe tomography (APT) is a technique capable of concurrently determining three dimensional material structure and chemistry at near atomic resolution which recently has been applied to investigating the apex regions of AFM tips. We present our investigations in utilizing APT to study material transfer phenomena during dry sliding experiments involving a Si AFM tip on Cu. The results show that Cu does transfer to the Si tip and has a dependency on both load and sliding distance. Comparisons are made to experiments by others on

the microscale and to molecular dynamics simulations of the wear of Cu. This study demonstrates the potential of APT in complementing AFM based studies to investigate nanotribological phenomena.

6.2 Introduction

During sliding of two materials it is well known that the interaction changes the material adjacent to the sliding interface. Many names have been given to this changed region: tribomaterial, Beilby layer, transfer layer, transfer film, glaze layer, tribolayer, white etching, and mechanically mixed layer. This layer is commonly different both structurally and chemically from the bulk material and can have great influence over the friction and wear properties of the interface [1]. Much work has been done on the macro and micro scales to try to characterize and understand how these layers develop and are structured. Focused ion beam lift out techniques combined with TEM and SEM have been used extensively to investigate the tribolayer formed on the substrate of pin on disk type experiments [2-4]. Raman spectroscopy has also been used to investigate the tribolayer on the disk side of the interface [5]. However quantitative investigation of the apex region of the pin is lacking especially on the nanometer scale. With the advent of miniaturized devices such as micro- and nano- electromechanical systems (MEMS/NEMS), surface forces and surface phenomena become dominant and can affect the reliability of the devices. Consequently a detailed assessment of

both sides of the interface is needed. Work has been done in molecular dynamics to model what happens on both sides at the atomic scale during sliding experiments [6-9], but thus far there has not been atomic scale experimental evidence to verify the models. Therefore a way to investigate the material transfer at the atomic level would be greatly beneficial.

Since its invention in the early 1980s atomic force microscopy (AFM) has become one of the most powerful tools in the fields of nanoscience and nanotechnology for the preparation and analysis of materials, nanostructures and their functionality [10-12]. AFM based techniques have especially been useful in the field of nanotribology, which is the study of friction, adhesion, lubrication and wear at contacts of nanometer sizes [10, 13-15]. Commonly measured nanotribological properties such as the coefficient of friction and wear rate are not intrinsic physical properties and can be strongly dependent on the specifics of the structure, physical, mechanical and chemical properties of the surface as well as the environment and instrumentation itself. Consequently obtaining a fundamental understanding of the phenomena requires careful experiments at well-defined surfaces. AFM studies can provide for this condition in which the tip simulates a single asperity contact. The use of probe shape characterizers and reconstruction algorithms allow precise evaluation and monitoring of the tip shape during experiments [16]. Techniques to reliably calibrate the normal and lateral spring constants of the cantilevers allow researchers to perform more accurate force measurements [17, 18], and calibration methods to perform

quantitative friction force microscopy are available [19, 20]. The materials and conditions studied are vast and continue to expand. AFM techniques thus allow accurate determination of the probe and contact dimensions during tribological measurements, which provide means to isolate tribological contributions from specific sources of interest.

While AFM based techniques have proved very useful in investigating nanotribological phenomena, a detailed assessment of the material structure and chemistry of the near apex region of the AFM tip can provide further insights. Few techniques exist that can provide this critical information. Specific areas that would directly benefit from this information include fabrication and friction/wear studies using AFM tips where material transfer and tip chemistry are of importance [21-23]. We recently reported that the material structure and chemistry of the near apex regions of commercial AFM tips can be successfully interrogated using three dimensional atom probe tomography down to the near atomic-scale [24].

Atom probe tomography (APT) is a technique capable of concurrently determining three dimensional material structure and chemistry at near atomic resolution which has seen expanding use in science and engineering fields [25-28]. APT uses the phenomenon of field evaporation, by which surface atoms of the specimen are ionized and subsequently desorbed by an electric field. A schematic of the APT instrumentation is shown in Fig. 1(a). In the work

presented here laser pulsing APT was used. In laser pulsing APT the field evaporation process is controlled by utilizing a cryogenically cooled (to reduce atomistic vibrations) needle-shaped specimen (to increase the electric field magnitude for evaporation) that is kept at a standing voltage while the tip apex is irradiated by a pulsed laser. The sample is traditionally prepared into a sharp needle shape with a tip radius on the order of 100nm by electropolishing a wire sample or using a focused ion beam to mill a tip [29, 30]. The standing voltage on the sample is kept close to the voltage needed for field evaporation, and the pulsed laser is used to increase the field just enough to allow one atom to field evaporate. The ionized atom is then repelled through a hole in the local electrode towards a wide-angle position-sensitive detector equipped with a time-of flight mass spectrometer with single atom sensitivity. Typical magnifications of the specimen at the detector in most APT instruments are about 5-6 million times. The lateral coordinates of the ions are calculated from the recorded impact position on the detector, whereas the depth coordinate along the specimen axis is calculated from the ion position in the evaporation sequence [31]. Finally, the spatial coordinates of each atom are combined with its elemental identity from the time of flight data to create a 3D computer reconstruction of the analysed region of the sample, as shown in Fig. 1(b). Spatial resolution is limited by small trajectory aberrations of the ions close to the specimen surface and is typically ~0.2 nm laterally and ~0.05 nm in the depth coordinate [32]. Detailed descriptions of the physical principle and performance of the method can be

found in various books and review articles [31, 33, 37, 39]. As a comparison, energy filtering transmission electron microscopy (EFTEM) can provide two-dimensional chemical mapping with about 1 nm lateral resolution, which is limited by signal to noise issues [33]. A direct comparison of identical calibration structures demonstrated that the spatial resolution of the local chemical analysis by APT exceeds that of the unprocessed EFTEM by a factor of 2 [34]. Thus APT is one of the highest resolution three dimensional nanoscale analysis tools presently available.

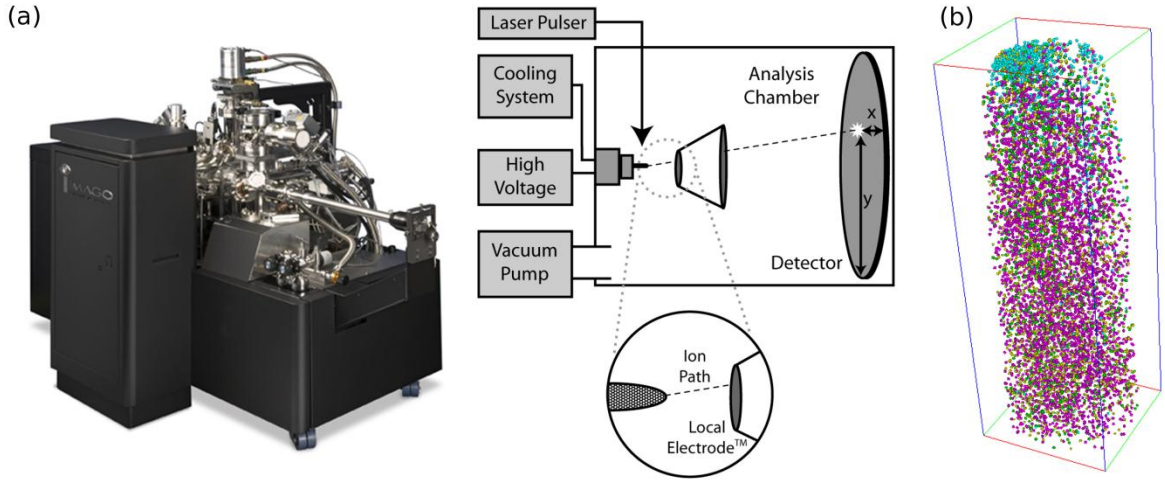

Fig. 1. (a) A commercial atom probe microscope (LEAP 3000X Si) and a schematic of the key elements associated in a measurement. (b) An example of a reconstructed stainless steel sample (reconstructed volume of 20x20x80nm) from atom probe data providing material structure and chemistry on the atomic

scale. Each sphere represents an atom while each color represents a different species.

Typical AFM tips have a conical tip with a tip radius less than 100nm that makes them suitable for analysis by atom probe tomography (APT). By utilizing an appropriate holder an AFM tip can be successfully examined using APT and 3D reconstructions of the atom positions in the near apex region of the AFM tip can be obtained, as demonstrated in our previous work [24]. In this paper we present our investigations in using APT to study material transfer during dry sliding experiments of silicon AFM tips against a polished copper substrate. To our knowledge this is the first attempt to experimentally evaluate transfer material on AFM tips as a result of dry sliding experiments at the nanoscale.

6.3 Experimental

Nanoscale dry sliding experiments were conducted using a Dimension 3100 AFM (Nanoscope IV, Veeco Instruments, Santa Barbara, CA) with commercially available Si(100) HAR5 and Aspire AFM tips (Nanoscience Instruments, Inc.) against a polished Cu surface. SEM micrographs of typical AFM tips used in the study are shown in Fig. 2(a) and (b). An important factor in successful APT experiments is for the sample to have a smooth tip with a

reasonably well-defined radius. Consequently, to reduce the risk of damage to the tip, the normal spring constant was found using Sader's method [18], and the sensitivity of each AFM tip was found using a recently reported method that uses a sharpened W wire as a contact point on the cantilever to avoid tip sample contact [35]. The tip radius of each AFM tip was then obtained prior to performing sliding experiments by reverse imaging [36-38] the tip in tapping mode using a tip characterizer (TGT1, NT-MDT). The tip radius is one of the parameters used in the software-based reconstruction of the atom positions in APT. Consequently the ability to determine a priori, a relatively accurate tip radius helps minimize errors in the reconstruction [31]. Figure 2(c) shows a typical AFM tip profile along with an approximate volume that is typically analysed and reconstructed in APT measurements. Tip radii are typically in the tens of nanometers. Dry sliding experiments with increasing load were carried out at normal forces of 100, 400, 700 and 1000nN using a new HAR5 tip for each experiment. For each experiment, the tip was scanned at 0.5 Hz (sliding speed of 2 μm/s) over a 2 μm scan length for a duration of 2 minutes. Sliding duration experiments were carried out at a normal force of 100nN on Aspire tips with sliding lengths of 0.24, 1.92, 3.84, 7.68, 15.36 and 30.72 mm which correspond to 0.5-128 min. length experiments. The length experiments were done at a scan speed of 2Hz (sliding speed of 8 μm/s) over a 2 μm scan length. All experiments were performed at ambient conditions (~25 °C, 45±5 %RH). The Cu surface was prepared by first wet sanding with 600 grit sandpaper followed by 1200 grit sandpaper using DI

water. Next it was polished using alpha alumina powder in DI water on a microcloth stepping down in size from 1 μm to 0.3 μm to 0.05 μm alpha alumina powder. A fresh microcloth was used for each size powder, and the Cu was rinsed with DI water between sizes. Finally the Cu was sonicated in distilled water. The final surface exhibited an RMS roughness value of ~12 nm as measured by a 5 μm x 5 μm AFM scan.

To investigate the chemistry and structure of material transfer the tips were analysed using a commercially available atom probe microscope (LEAP 3000X Si, Cameca Instruments Inc., Madison WI) in laser mode. The AFM tips were loaded into the instrument using a clip holder (Cameca Instruments Inc.) which allowed analysis of the AFM tip without the need for permanent mounting. The samples were loaded into the atom probe microscope (vacuum) and APT was conducted as soon as running pressure was reached (<6 hours). Experiments were conducted at 2x10-11 Torr or less, 70 K or less, 200 kHz, 0.3nJ laser pulse and 160 mm flight path. Reconstruction of the APT runs was done using IVAS software (Cameca Instruments Inc.).

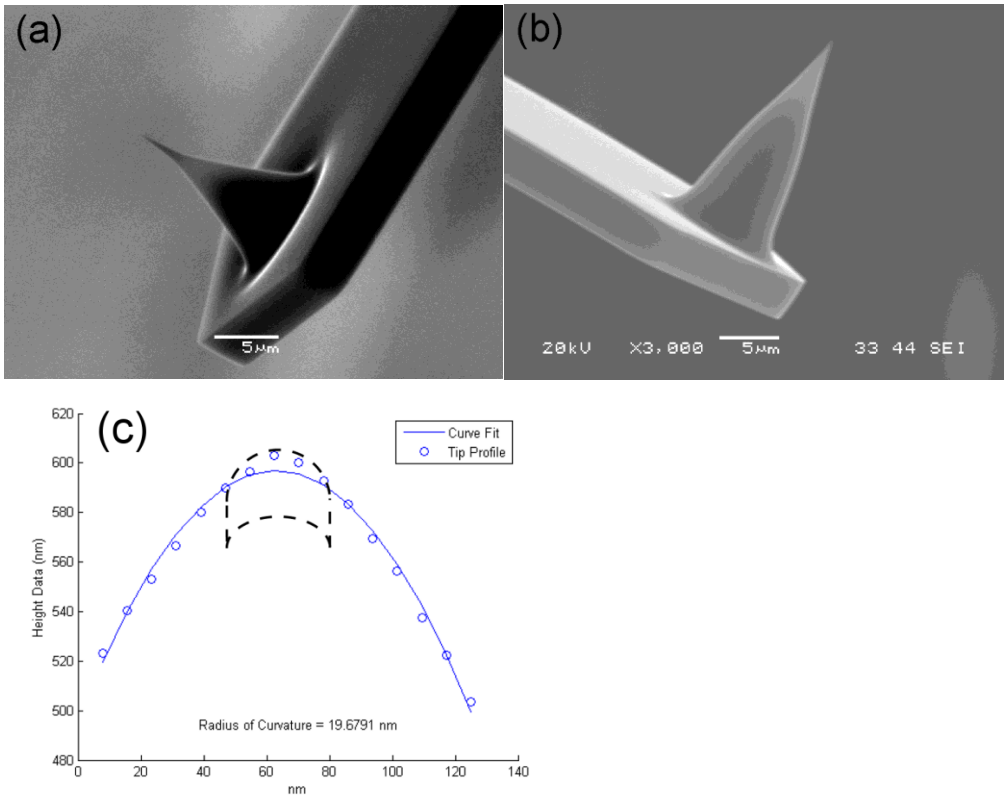

Fig. 2. SEM image of a typical commercial Si(100) HAR5 (a) and Aspire (b) AFM tip used in the experiments. (c) An example of the tip profile obtained via scanning a tip characterizer sample and subsequent reverse imaging in order to determine the radius. The dashed box highlights the approximate area of the reconstruction volume in APT analysis.

6.4 Discussion

Most nanoscale wear studies using the AFM report the observed depth of the wear area and the results often support a wear process in which the depth increases with normal load [10, 15, 39-42]. This information is easily obtained by imaging the scanned (worn) region using the same probe used to perform the wear experiment but at a lower imaging normal load. In our experiments since the objective was to determine the material transfer onto the probe, we did not perform this step. However a separate set of experiments was done at the same conditions to evaluate the wear trench. The results of the average wear trench depth verses normal load and number of cycles are shown in Fig. 3(a) and (b) respectively. Both increasing load and increasing cycles show the depth of the wear trench developed increased. This agrees well with trends others have seen for Cu wear dependence on both normal load and cycles [43-45].

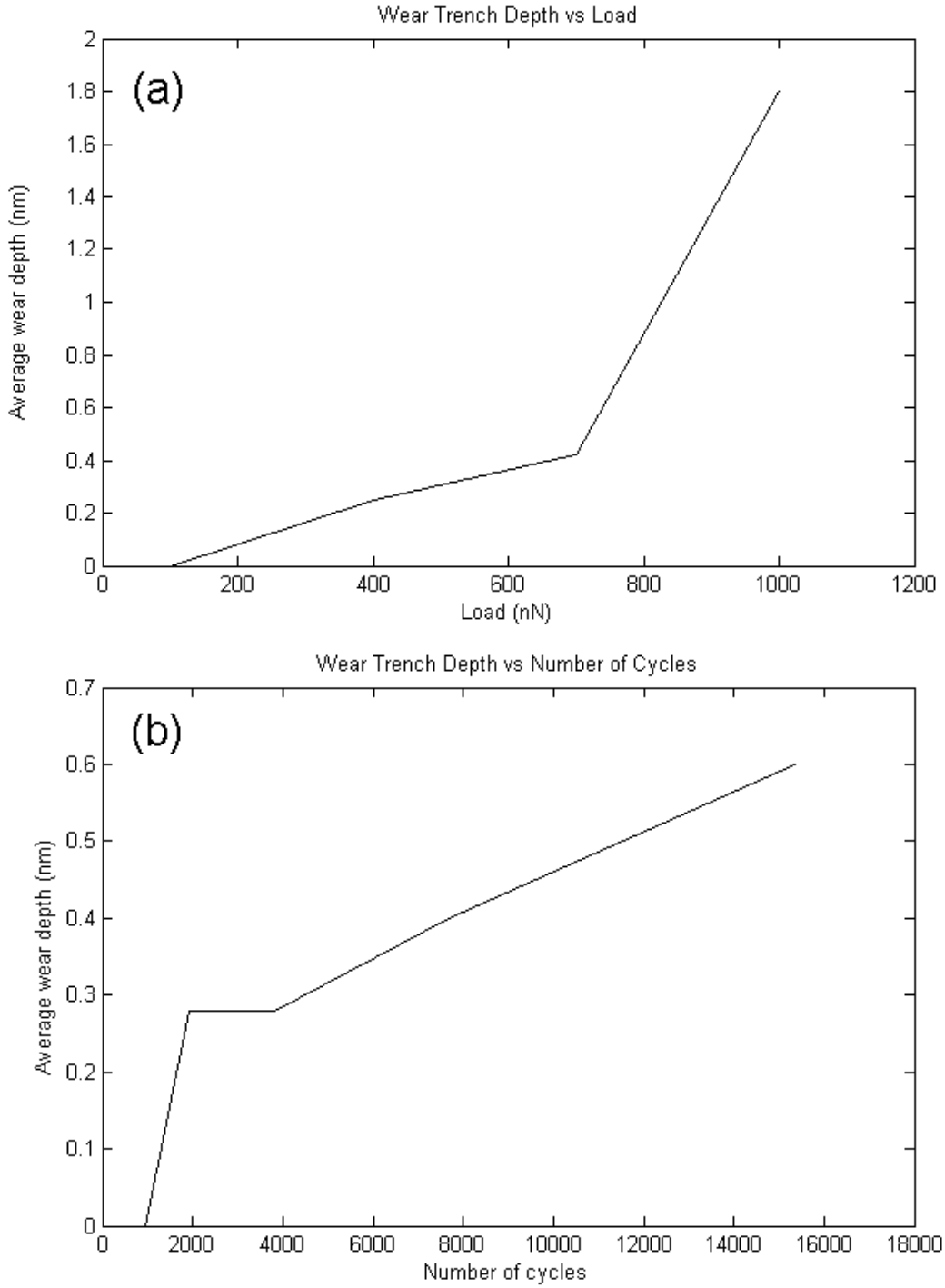

Fig. 3. Graphs showing the average wear depth vs increasing load (a) and number of cycles (b).

APT analysis of the tips subjected to all four loads and all six wear lengths show the presence of Cu. Figure 4(a) shows a typical mass spectrum of an APT run on a tip subject to sliding and the easily identifiable Si and Cu peaks. The Cu peaks have been highlighted for clarity. As a comparison, the mass spectrum of an unused Si tip shows no presence of Cu (Fig. 4(b)). The data therefore is indicative of material transfer due to contact during sliding. We note that both the Cu and Si peaks are well above the noise floor and that the presence of distinct and sharp Cu peaks in the mass spectrum also indicates that the Cu adhered to the silicon AFM tip strongly enough to field evaporate in a controlled manner.

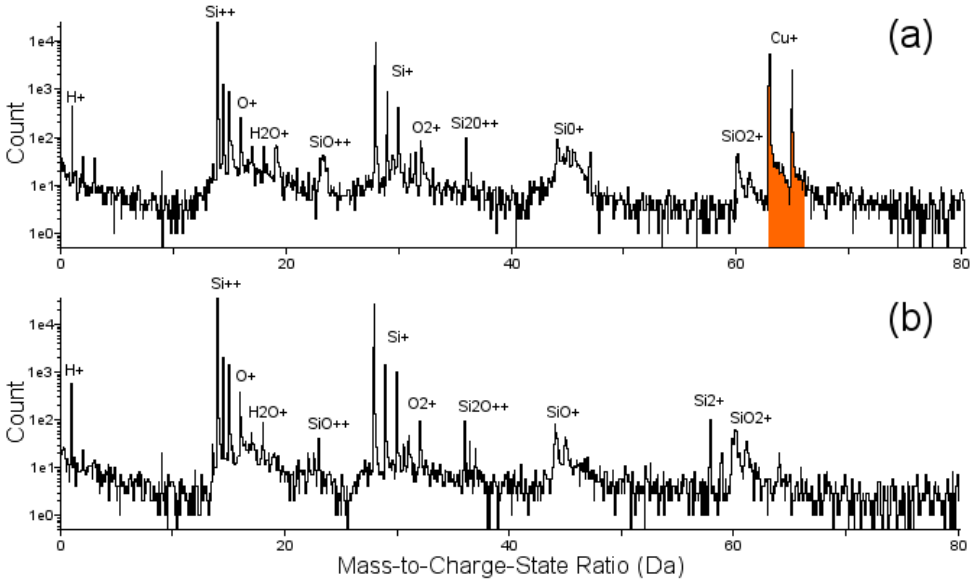

Fig. 4. Typical mass spectrum from an APT run on an AFM tip used in a dry sliding experiment on Cu (a) and an unused AFM tip for comparison (b).

The reconstructions of the Si tips from the APT runs were analyzed to discern the distribution of the transferred material. The field of view for the APT reconstruction is a truncated cone with a starting radius of about 15 nm that penetrates down the axis of the AFM tip. A view down the axis of the reconstruction (top view) of the top 10 nm of a representative reconstruction showing the distribution of Cu are shown in Fig. 5. The silicon atoms are not shown for ease of interpretation of the image. It is readily apparent that the Cu transferred does not exist as a continuous film on the surface; rather the Cu atoms appear to have transferred in clumps. The non-uniform distribution was seen in all loads and sliding distances. This non-uniform distribution was predicted in recent molecular dynamics modeling of Cu on Fe during sliding [7, 8]. It was seen in the simulations that Cu near the interface formed areas of BCC Cu and when the surfaces where separated these regions adhered to the Fe. We believe that a similar process for material transfer is happening here, however the amount of Cu transferred was not enough to find information in the reconstruction about Cu's crystal structure.

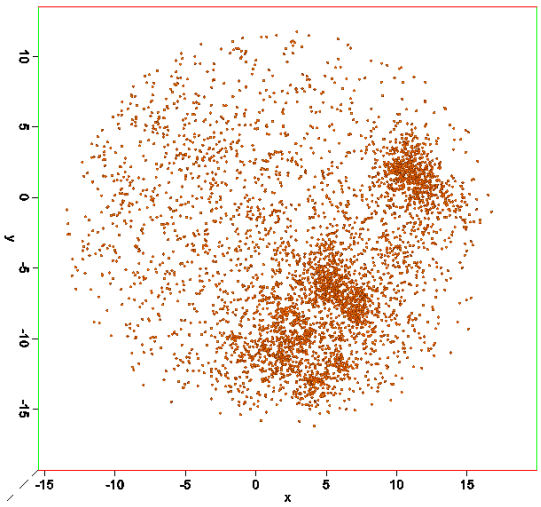

Fig. 5. Top view of a typical reconstruction showing the uneven distribution of Cu atoms on the AFM tip apex (distances in nm). Si atoms are not shown for ease of interpretation.

The reconstructions also allow the investigation of atomic percentages of the elements of interest. Fig. 6(a) shows the total amount of Cu (atomic %) present in the top 5 nm of the reconstructions as a function of normal load during sliding. Since all other parameters were held constant, the observed differences can be attributed to the change in normal load. While the amount of Cu transferred increases with the first two normal loads, it peaks at 400nN and decreases in the last two normal loads. This is contrary to what would be expected from the increase of wear trench depth with load. We believe this trend can be explained by the increasing load aiding in transfer until at higher loads the

transferred material is pulled back off of the AFM tip. Another explanation could be a transition from an adhesive to abrasive wear regime at the higher loads. However the role of normal and shear stresses that manifest during the sliding process on the transfer process is still not clearly understood and further investigation is required to confirm and explain the normal load trend seen here.

The amount of Cu present in the top 5 nm of the reconstruction as a function of sliding distance is shown in Fig. 6(b). The top 5 nm was chosen as a standard because it captured all the Cu transferred for every run. It can be seen that with increasing sliding distance there is an upward trend in the amount of Cu transferred. A line has been added to help visualize the trend. The increased amount of contact time seems to have allowed more Cu to transfer onto the AFM tip. This increasing trend agrees well with qualitative work done on the microscale by Zhang et al who saw an increasing trend in the amount of Cu transferred to a stainless steel ball during increasing sliding distance at the microscale [46]. Therefore what has been seen at the multiple asperity level seems to hold true at the single asperity level.

It is worth noting that experiments were done with an AFM tip pressed against the Cu without sliding for similar load and time without any Cu seen to transfer. Also tips used in intermittent contact mode (sometimes referred to as tapping mode) on Cu did not show Cu material transfer. From this it seems that material transfer only happens in the presence of lateral stress.

A final set of experiments was conducted on Ag with the same 100nN load and scanning parameters as the increasing scanning distance experiments on Cu. It was seen in the APT analysis that Ag did transfer to the AFM tip in all samples that survived. However a trend in the amount transferred was unable to be determined due to a high rate of sample fractures during APT.

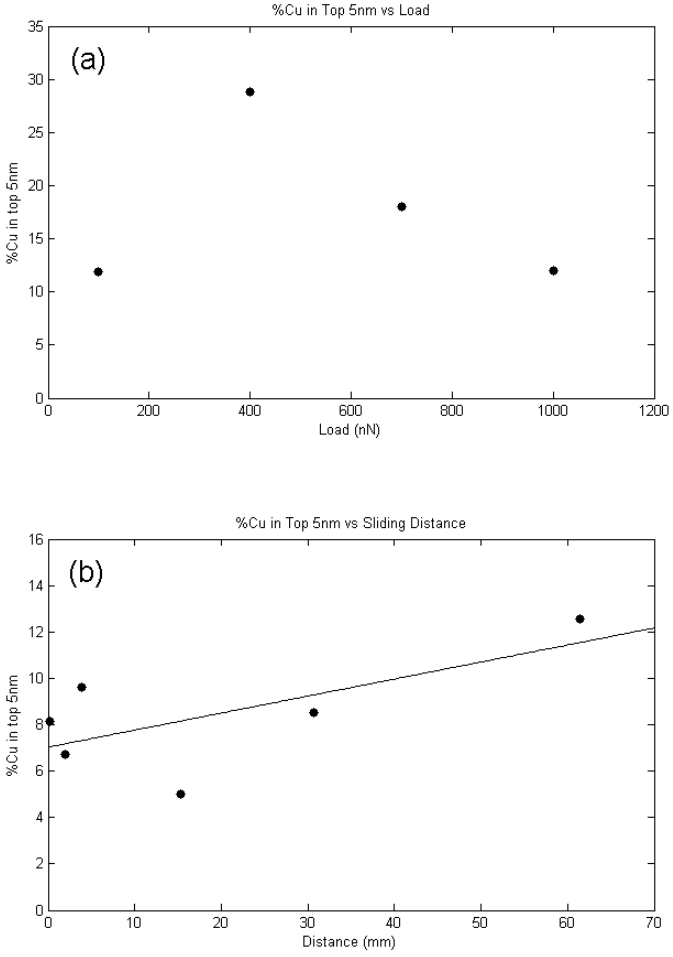

Fig. 6. Graphs showing the amount of Cu in the tip 5 nm of the APT reconstruction as a measure of the amount of Cu transferred to the tip during dry sliding on Cu under varying load (a) and varying sliding distance (b).

6.5 Conclusions

This study represents the first attempt to investigate at the atomic scale material transfer onto an AFM tip subjected to sliding experiments. APT was used to investigate material transfer during dry sliding experiments involving a Si AFM tip on Cu. The results show that Cu transfers to the Si tip in a non-uniform manner rather than existing as a distinct layer at the surface. The amount of Cu transferred depends on both the normal load and sliding distance. The results confirmed experimentally what has been seen in molecular dynamics modelling and what has been seen on the microscale. This study thus demonstrates the potential of APT in complementing AFM based studies to interrogate nanotribological and other interfacial phenomena at the nanoscale by utilizing APT for atom-scale analysis of the near-apex regions of the AFM probe.

Acknowledgements

Partial funding for this study was provided by grants from the National Science Foundation (Grant no. 0932573) and the W.M. Keck Foundation.

References

[1] D.A. Rigney, S. Karthikeyan, The Evolution of Tribomaterial During Sliding: A Brief Introduction, Tribol. Lett., 39 (2010) 3-7.

[2] A. Emge, S. Karthikeyan, D.A. Rigney, The effects of sliding velocity and sliding time on nanocrystalline tribolayer development and properties in copper, Wear, 267 (2009) 562-567.

[3] R. Schouwenaars, V.H. Jacobo, A. Ortiz, Microstructural aspects of wear in soft tribological alloys, Wear, 263 (2007) 727-735.

[4] R. Schouwenaars, V.H. Jacobo, S. Cerrud, A. Ortiz, Tribolayer formation as a functionally self-grading process in soft anti-friction alloys, in: O. VanderBiest, M. Gasik, J. Vleugels (Eds.) Functionally Graded Materials Viii, Trans Tech Publications Ltd, Zurich-Uetikon, 2005, pp. 531-537.

[5] J.V. Pimentel, T. Polcar, M. Evaristo, A. Cavaleiro, Examination of the tribolayer formation of a self-lubricant W-S-C sputtered coating, Tribol. Int., 47 (2012) 188-193.

[6] H.J. Kim, W.K. Kim, M.L. Falk, D.A. Rigney, MD simulations of microstructure evolution during high-velocity sliding between crystalline materials, Tribol. Lett., 28 (2007) 299-306.

[7] E.Q. Lin, L.S. Niu, H.J. Shi, Z. Duan, Molecular dynamics simulation of nano-scale interfacial friction characteristic for different tribopair systems, Appl. Surf. Sci., 258 (2012) 2022-2028.

[8] S. Karthikeyan, A. Agrawal, D.A. Rigney, Molecular dynamics simulations of sliding in an Fe-Cu tribopair system, Wear, 267 (2009) 1166-1176.

[9] J.E. Hammerberg, B.L. Holian, T.C. Germann, R. Ravelo, Nonequilibrium molecular dynamics simulations of metallic friction at Ta/Al and Cu/Ag interfaces, Metall. Mater. Trans. A-Phys. Metall. Mater. Sci., 35A (2004) 2741-2745.

[10] B. Bhushan, J.N. Israelachvili, U. Landman, NANOTRIBOLOGY - FRICTION, WEAR AND LUBRICATION AT THE ATOMIC-SCALE, Nature, 374 (1995) 607-616.

[11] P.T. Lillehei, L.A. Bottomley, Scanning probe microscopy, Analytical Chemistry, 72 (2000) 189R-196R.

[12] J. Loos, The art of SPM: Scanning probe microscopy in materials science, Advanced Materials, 17 (2005) 1821-1833.

[13] R.W. Carpick, M. Salmeron, Scratching the surface: Fundamental investigations of tribology with atomic force microscopy, Chemical Reviews, 97 (1997) 1163-1194.

[14] Bhushan, Handbook of Micro/Nanotribology Second Edition, 1998.

[15] I. Szlufarska, M. Chandross, R.W. Carpick, Recent advances in single-asperity nanotribology, J. Phys. D-Appl. Phys., 41 (2008) 39.

[16] K.S.K. Karuppiah, S. Sundararajan, Z.H. Xu, X.D. Li, The effect of protein adsorption on the friction behavior of ultra-high molecular weight polyethylene, Tribology Letters, 22 (2006) 181-188.

[17] A. Torii, M. Sasaki, K. Hane, S. Okuma, A method for determining the spring constant of cantilevers for atomic force microscopy, Measurement Science & Technology, 7 (1996) 179-184.

[18] J.E. Sader, J.W.M. Chon, P. Mulvaney, Calibration of rectangular atomic force microscope cantilevers, Rev. Sci. Instrum., 70 (1999) 3967-3969.

[19] J.-A. Ruan, B. Bhushan, Atomic-scale friction measurements using friction-force microscopy. Part I. General principles and new measurement techniques, Journal of Tribology, 116 (1994) 378-388.

[20] D.F. Ogletree, R.W. Carpick, M. Salmeron, Calibration of frictional forces in atomic force microscopy, Review of Scientific Instruments, 67 (1996) 3298-3306.

[21] K.H. Chung, D.E. Kim, Wear characteristics of diamond-coated atomic force microscope probe, Ultramicroscopy, 108 (2007) 1-10.

[22] K.S.K. Karuppiah, A.L. Bruck, S. Sundararajan, Evaluation of Friction Behavior and Its Contact-Area Dependence at the Micro- and Nano-Scales, Tribology Letters, 36 (2009) 259-267.

[23] K. Tanaka, M. Yoshimura, K. Ueda, High-Resolution Magnetic Force Microscopy Using Carbon Nanotube Probes Fabricated Directly by Microwave Plasma-Enhanced Chemical Vapor Deposition, Journal of Nanomaterials, (2009).

[24] C. Tourek, S. Sundararajan, Study of Atomic Force Microscopy Probes Using a Local Electrode Atom Probe Microscope, in, Cambridge Journals Online, 2009, pp. 290-291.

[25] T.F. Kelly, M.K. Miller, Invited review article: Atom probe tomography, Rev. Sci. Instrum., 78 (2007) 20.

[26] D.N. Seidman, Three-dimensional atom-probe tomography: Advances and applications, Ann. Rev. Mater. Res., 37 (2007) 127-158.

[27] T.F. Kelly, D.J. Larson, K. Thompson, R.L. Alvis, J.H. Bunton, J.D. Olson, B.P. Gorman, Atom probe tomography of electronic materials, Ann. Rev. Mater. Res., 37 (2007) 681-727.

[28] F. Danoix, P. Auger, Atom probe studies of the Fe-Cr system and stainless steels aged at intermediate temperature: A review, Mater. Charact., 44 (2000) 177-201.

[29] M.K. Miller, K.F. Russell, G.B. Thompson, Strategies for fabricating atom probe specimens with a dual beam FIB, Ultramicroscopy, 102 (2005) 287-298.

[30] G.B. Thompson, M.K. Miller, H.L. Fraser, Some aspects of atom probe specimen preparation and analysis of thin film materials, Ultramicroscopy, 100 (2004) 25-34.

[31] M.K. Miller, Atom Probe Tomography Analysis at the Atomic Level, Kluwer Academic/Plenum Publishers, New York, 2000.

[32] M.K. Miller, Interface analysis with the three-dimensional atom probe, Surface and Interface Analysis, 31 (2001) 593-598.

[33] W. Grogger, B. Schaffer, K.M. Krishnan, F. Hofer, Energy-filtering TEM at high magnification: spatial resolution and detection limits, Ultramicroscopy, 96 (2003) 481-489.

[34] P. Stender, T. Heil, H. Kohl, G. Schmitz, Quantitative comparison of energy-filtering transmission electron microscopy and atom probe tomography, Ultramicroscopy, 109 (2009) 612-618.

[35] C.J. Tourek, S. Sundararajan, An alternative method to determining optical lever sensitivity in atomic force microscopy without tip-sample contact, Review of Scientific Instruments, 81 073711-073715.

[36] V. Bykov, A. Gologanov, V. Shevyakov, Test structure for SPM tip shape deconvolution, Appl. Phys. A-Mater. Sci. Process., 66 (1998) 499-502.

[37] J.S. Villarrubia, Algorithms for scanned probe microscope image simulation, surface reconstruction, and tip estimation, J. Res. Natl. Inst. Stand. Technol., 102 (1997) 425-454.

[38] P.M. Williams, K.M. Shakesheff, M.C. Davies, D.E. Jackson, C.J. Roberts, S.J.B. Tendler, Blind reconstruction of scanning probe image data, Journal of Vacuum Science and Technology B, 14 (1996) 1557-1562.

[39] B. Bhushan, Nanoscale tribophysics and tribomechanics, Wear, 225 (1999) 465-492.

[40] P.R. Chidambaram, C. Bowen, S. Chakravarthi, C. Machala, R. Wise, Fundamentals of silicon material properties for successful exploitation of strain engineering in modern CMOS manufacturing, IEEE Trans. Electron Devices, 53 (2006) 944-964.

[41] K. Degiampietro, R. Colaco, Nanoabrasive wear induced by an AFM diamond tip on stainless steel, Wear, 263 (2007) 1579-1584.

[42] S. Sundararajan, B. Bhushan, Micro/nanotribology of ultra-thin hard amorphous carbon coatings using atomic force friction force microscopy, Wear, 225 (1999) 678-689.

[43] K.H. Chung, D.E. Kim, Fundamental investigation of micro wear rate using an atomic force microscope, Tribol. Lett., 15 (2003) 135-144.

[44] M. Curry, X. Li, F. Huang, M.L. Weaver, S.C. Street, A tribological study of kinetically influenced ultrathin Au and Cu metal overlayers grown on dendrimer mediated Si, Tribol. Lett., 25 (2007) 133-140.

[45] W.E. Fu, C.C.A. Chen, K.W. Huang, Y.Q. Chang, Material removal mechanism of Cu-CMP studied by nano-scratching under various environmental conditions, Wear, 278 (2012) 87-93.

[46] Y.S. Zhang, K. Wang, Z. Han, K. Lu, Transfer behavior in low-amplitude oscillating wear of nanocrystalline copper under oil lubrication, J. Mater. Res., 23 (2008) 150-159.

CHAPTER 7. CONCLUSIONS

Atom Scale Characterization of the Near Apex Region of an Atomic Force Microscope Tip

APT analysis was successfully shown as a viable technique to obtain near atomic scale information of the material structure and chemistry of the near-apex regions of AFM tips. To demonstrate the technique AFM tips were analyzed as received and compared to a known APT sample. The results showed the ability to successfully run the AFM tips in the atom probe microscope and detect crystal structure in the reconstructions. It was found through FEA modeling that using AFM tips with a spring stiffness greater than 25N/m reduced the bending in the electric field present in during APT. AFM tips and presharpend microtip samples where coated with Cu to demonstrate the ability to investigate a thin film on the AFM tip by using APT. The results were compared to TEM and showed good agreement. The findings open up new avenues of investigation for AFM-related research, especially in characterizing material transferred or generated on AFM tips.

Detection and analysis of the native oxide layer on the near apex region of atomic force microscope tips using laser pulsed atom probe tomography

Laser pulsed APT was used to investigate the structure and chemistry of the native oxide layer that is present on as received AFM tips at the near-atomic scale. Three types of dry etched commercially available Si AFM tips were assessed, and the native oxide layer was found to be 0.5, 0.7, and 1.5nm on HAR5, Aspire, and NSC15 AFM tips respectively. In addition the NSC15 tips showed aluminum, likely from the backside coating process. The native oxide layer was shown to be readily detected in laser pulsed mode, but not in voltage pulsed mode. Therefore studies where the oxide layer is of importance should be conducted in laser pulsed mode.

Analysis of the near-apex regions of scanning probe microscopy tips using atom probe tomography

APT of AFM tips was extended to investigating the near-apex regions of several commercially available AFM tips. Conical Si tips coated with Si_3N_4 or DLC were successfully analyzed in pulsed laser mode in the atom probe microscope. The Si_3N_4 coated tips required a higher laser power than uncoated Si to induce field evaporation and tended to field evaporate in various Si_xN_y compounds. The DLC coated tips also required a high laser power along with a higher temperature to achieve consistent field evaporation. The evaporation of

the DLC exhibited mostly C_3^{++}, C^{+} and C^{++} species however the coating also showed presence of hydrocarbons at higher concentrations at evenly spaced intervals through the coating thickness. In almost all the runs on the coated tips' stable field evaporation stopped when the interface was reached. This was caused by the large difference in the fields needed to evaporate the coatings compared to the Si substrate and rendered imaging and analysis of the interface difficult. Constant diameter Ag_2Ga needle tips were also readily analyzed and showed an overall composition close to bulk Ag_2Ga. However the reconstruction showed a segregated structure of Ga rich and depleted areas. This work demonstrates that the power of APT can be applied to multiple coatings and chemistries that are used throughout the AFM community giving a very powerful tool to analyze surface and interfacial phenomena that occur at the near-apex regions of SPM tips.

An alternative method to determining optical lever sensitivity in atomic force microscopy without tip-sample contact

It was found that the traditional way to measure the optical sensitivity of an AFM cantilever by pressing against a hard surface and measuring the slope of the force curve can damage sharp tips. This damage can affect the resolution of the measurements and impact future experiments. A novel method was shown to calculate the optical sensitivity without tip sample contact. Instead a reusable tungsten wire was used to generate a point contact directly onto the cantilever.

Comparisons between the new method and traditional method showed a difference of less than 12% for rectangular cantilevers. The new method offers a simple alternative approach without need to modify the AFM which is especially useful for studies where the sharpness of the AFM tip cannot be compromised.

Characterization of material transfer onto an atomic force microscope tip resulting from nanoscale dry sliding using atom probe tomography

Material at the interface of two materials in sliding is well known to undergo chemical and structural changes. There has been much work done to analyze the flat interface of pin on disk type experiments, however investigation of the apex region of the pin is lacking especially on the nanometer scale. To investigate APT was used to analyze the material transferred during dry sliding experiments involving a Si AFM tip on Cu. The results show that Cu transfers to the Si tip in a non-uniform manner rather than existing as a distinct layer at the surface agreeing with what was seen in molecular dynamics simulations [1, 2]. The amount of Cu transferred was found to depend on both normal load and sliding distance agreeing with observations of Cu transfer at the microscale [3]. This study thus demonstrates the potential of APT in complementing AFM based studies to interrogate nanotribological and other interfacial phenomena at the nanoscale by utilizing APT for atom-scale analysis of the near-apex regions of the AFM probe.

Future study recommendations

The techniques developed here enable the analysis of transferred material on the near-apex region of AFM tips at the nano-scale by APT. By combining the work done on hard coated AFM tips with investigating transferred material, the techniques could be expanded to wear on hard materials. For example, materials used in fuel cells or catalysts could be analyzed to investigate the durability and life expectancy of the device. Also of interest would be wear in fluid, especially investigating wear on materials used in biological implants.

References

1. Karthikeyan, S., A. Agrawal, and D.A. Rigney, Molecular dynamics simulations of sliding in an Fe-Cu tribopair system. Wear, 2009. 267(5-8): p. 1166-1176.

2. Lin, E.Q., et al., Molecular dynamics simulation of nano-scale interfacial friction characteristic for different tribopair systems. Applied Surface Science, 2012. 258(6): p. 2022-2028.

3. Zhang, Y.S., et al., Transfer behavior in low-amplitude oscillating wear of nanocrystalline copper under oil lubrication. Journal of Materials Research, 2008. 23(1): p. 150-159.